The Relationship of Surface Pressure Features to the Precipitation and Airflow Structure of an Intense Midlatitude Squall Line

RICHARD H. JOHNSON AND PAUL J. HAMILTON

Department of Atmospheric Science, Colorado State University, Fort Collins, Colorado

(Manuscript received 23 September 1987, in final form 7 January 1988)

ABSTRACT

Observations from the Oklahoma–Kansas Preliminary Regional Experiment for STORM-Central (OK PRESTORM) have been used to document the surface pressure features accompanying an intense midlatitude squall line with trailing stratiform precipitation. Three well-known features are observed: a pre-squall mesolow, a squall mesohigh and a wake low. Particular attention is given to the wake low, its life cycle and association with the trailing stratiform portion of the squall line.

During the formative stage, the pressure field to the rear of the squall line mesohigh is relatively flat with only weak stratiform precipitation present. As the squall line enters the developing-to-mature stages, a pronounced wake low appears at the back edge of the surface stratiform precipitation area. The squall line at this time is characterized by a strong rear-inflow jet, descending from the upper troposphere, as far as 500 km behind the leading convective line, to the lower troposphere just behind the line. The trailing stratiform cloud constitutes a significant part of the squall-line water budget, contributing 29% of the total squall line precipitation over a 400 km by 500 km mesonetwork area experiencing its passage. During the mature-to-dissipating stages, the trailing stratiform region splits into two segments, as does the wake low, with each low pressure center hugging the back edge of the stratiform segments. A composite analysis of rawinsonde data at this time shows strong warming and drying in the lower troposphere at the back edge of the stratiform regions.

Based on the results of this study, it is proposed that the wake low, which can be attributed to subsidence warming, is a surface manifestation of the descending rear-inflow jet and that the warming is maximized at the back edge of the trailing stratiform precipitation area where there is insufficient sublimation and evaporative cooling to offset adiabatic warming.

1. Introduction

Lines or bands of deep, precipitating convective cells (here referred to as *squall lines*) in the midlatitudes and tropics have long been known to produce significant disturbances to the surface pressure field in their vicinity. Frequently, during their mature stage, squall lines have attendant areas of light, stratiform rain. Depending on the environmental wind shear, the stratiform precipitation areas may be found ahead of or straddling the convective line (e.g., Newton and Fankhauser 1964 and Newton 1966, for midlatitude lines; Houze and Rappaport 1984 for tropical lines) or to the rear of or trailing the convective line (Newton 1950; Fujita 1955; Pedgley 1962; Sanders and Emanuel 1977; Ogura and Liou 1980; Smull and Houze 1985; Srivastava et al. 1986; Leary and Rappaport 1987 for midlatitude lines, and Zipser 1969, 1977; Houze 1977; Gamache and Houze 1982, 1983, 1985; Chong et al. 1987 for tropical lines). This study is concerned with surface pressure variations accompanying the 10–11 June 1985 squall line observed in the Oklahoma–Kansas Preliminary Regional Experiment for STORM[1]-Central (OK PRESTORM; Cunning 1986). This squall line contained a trailing-type stratiform precipitation area (Fujita 1955).

Several prominent features of the wind field of midlatitude squall lines with trailing stratiform regions have been recently studied in detail by Ogura and Liou (1980), Smull and Houze (1985, 1987a,b) and Srivastava et al. (1986). One is a pronounced front-to-rear relative flow sloping upward from low levels ahead of the surface gust front to high levels in the rear. This current serves to transport hydrometeors rearward from convective line to the stratiform region where they eventually contribute to the precipitation there (Smull and Houze 1985; Rutledge and Houze 1987). Additional precipitation in the stratiform region can be attributed to successive incorporation of old cells from the convective line and the in situ generation of new condensate by a mesoscale updraft (Brown 1979; Gamache and Houze 1982; Rutledge 1986; Smull and Houze 1987a; Rutledge and Houze 1987).

Beneath this sloping updraft resides a layer of system-

Corresponding author address: Dr. Richard H. Johnson, Dept. of Atmospheric Science, Colorado State University, Fort Collins, CO 80523.

[1] STORM: STormscale Operational and Research Meteorology.

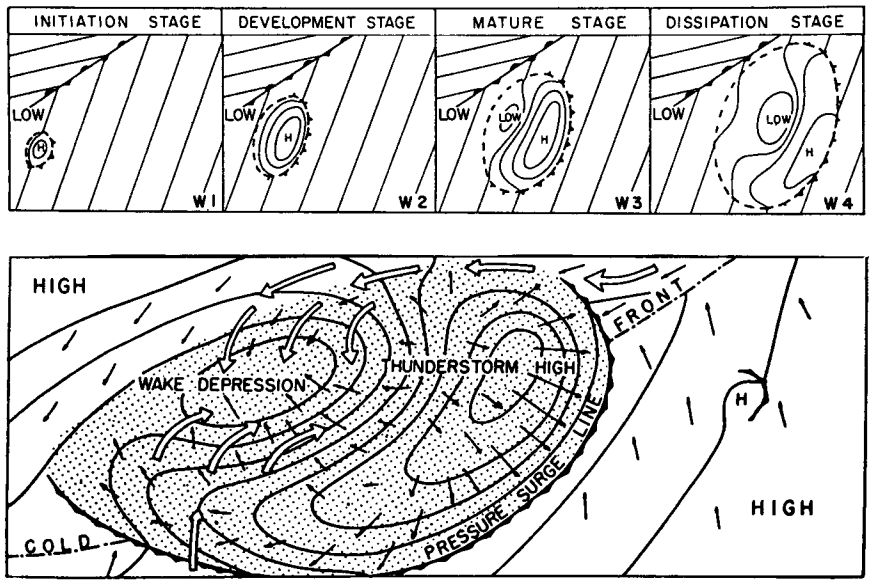

FIG. 1. Isobar patterns for four stages of squall-mesosystems (top, from Fujita 1963). The W designates warm sector type system. Schematic of surface pressure field in a squall-line thunderstorm (bottom, from Fujita 1955). Small arrows indicate surface wind; large arrows relative flow into the wake. Stippling indicates extent of precipitation-cooled air.

relative rear-to-front flow (termed a *rear-inflow jet* by Smull and Houze 1987b). The studies of Srivastava et al. (1986), Smull and Houze (1987b) and Chong et al. (1987) indicate that this current descends toward the convective line through the stratiform region. The rear-inflow jet and associated mesoscale descent, as will be seen, appear to play a prominent role in determining the surface pressure distribution to the rear of the squall line. A well defined front-to-rear flow and descending rear-inflow jet were present in the 10–11 June 1985 squall line, as recently described by Rutledge et al. (1988).

Three primary features are typically identified in the surface pressure field for squall lines accompanied by trailing stratiform regions: a pre-squall mesolow, a squall line mesohigh and a trailing wake low[2] (Fujita 1955; Pedgley 1962; Schaefer et al. 1985). They can be observed with prefrontal, frontal or postfrontal squall lines, but are probably most clearly distinguishable in prefrontal lines (the case studied here).

A schematic illustrating two of these three surface pressure features, the mesohigh and the wake low, over the life cycle of a prefrontal squall line is presented in Fig. 1 (top, from Fujita 1963). Four stages are identified by Fujita.

1) *Initiation stage.* A small mesohigh forms and develops.

2) *Development stage.* Horizontal dimensions increase to over 150 km, yet no mesolow appears inside the system.

3) *Mature stage.* Showers reach their maximum intensities, and a mesolow develops behind them.

4) *Dissipation stage.* The wake low reaches the minimum deficit pressure and showers disintegrate.

This sequence fits the surface pressure pattern quite well over the life cycle of the squall line reported in this paper, except that in our case a pre-squall mesolow was also observed and, in addition, the wake low split into two segments (to be illustrated later). Pedgley (1962) defined a similar life cycle of the squall line pressure field using a three-stage schematic.

A schematic of the surface pressure and wind field during the mature stage of a cold frontal squall line is shown in Fig. 1 (bottom, from Fujita 1955). The wake low is positioned toward the rear of the area of precipitation-cooled air (stippling) with surface flow converging into it. A surface diffluence axis occurs to the rear of the thunderstorm mesohigh center with air accelerating through the mesohigh toward the leading convective line. The results of our analysis, when incorporated with those in the earlier works cited above, yield a somewhat revised depiction of the pressure, wind and precipitation structure in the region of the trailing wake low. Specifically, it is the purpose of our study to establish an association between the mesoscale pressure features, particularly the wake low, and the cloud, precipitation and air flow characteristics of the squall line, thereby providing some insight into their formation and maintenance mechanisms.

[2] Other names have been used for these features; for the mesohigh: thunderstorm high, pressure dome and bubble high, and for the wake low: wake depression, mesodepression, wake mesolow and thunderstorm wake.

Based on the analysis presented herein, we propose that the wake low, which can be attributed to subsidence warming (Williams 1963; Zipser 1977), is a surface manifestation of the descending rear-inflow jet and that the warming is maximized at the back edge of the precipitation area where the cooling associated with sublimation and evaporation is small and insufficient to offset strong adiabatic warming. These processes will be examined in detail using the comprehensive dataset obtained during the passage of the 10–11 June squall line.

2. Mechanisms for squall-line surface pressure perturbations

a. The pre-squall mesolow

This feature, which is not a major focus of our study, has been attributed by Hoxit et al. (1976) to convectively induced subsidence warming in the mid-to-upper troposphere ahead of squall lines. Observational studies (e.g., Fankhauser 1974; Sanders and Paine 1975; Gamache and Houze 1982) confirm the existence of pre-squall subsidence. The modeling study of Fritsch and Chappell (1980) provides strong evidence in support of the Hoxit et al. (1976) explanation for this feature. Warm advection may also play some role in the mesolow formation (Schaefer et al. 1985), although it is likely secondary.

b. The squall mesohigh

The thunderstorm mesohigh was clearly identified in the "Thunderstorm Project" measurements of Byers and Braham (1949) and is located just to the rear of the region of the squall line heavy precipitation and convective downdrafts. Sawyer (1946) and Fujita (1959) attributed the mesohigh primarily to rainfall evaporation, although Fujita noted that in some circumstances, there may be an additional (nonhydrostatic) contribution to surface pressure rise by the impact of the precipitation downdraft with the ground. Hydrometeor loading can also contribute to the mesohigh (e.g., Sanders and Emanuel 1977). It seems likely that melting and sensible cooling by hail may also strengthen the mesohigh in some circumstances (Fujita 1959).

c. The wake low

The wake low has for years been clearly identified as a prominent feature of mature squall lines (Brunk 1953; Fujita 1955, 1963; Pedgley 1962; Williams 1953, 1963), but the dynamical mechanism for its formation has been elusive. According to Atkinson (1981, p. 356), "the wake low is far less well documented than the high." Indeed, a full explanation of the dynamics of the wake low has not yet been presented, although a number of authors have convincingly demonstrated that it owes its existence to strong subsidence warming behind the squall line.

Williams (1963) was the first to demonstrate in a quantitative way that subsidence warming can account for the observed pressure deficit in the wake low. His analysis of the thunderstorm wake of 4 May 1961, indicates a descending warm, dry current to the rear of a convective line with warm air, in this case, actually reaching the surface.[3] Williams, however, was not able to establish the cause of this circulation nor was the relationship between the wake low and the trailing precipitation region investigated.

A warm, dry lower troposphere is a common feature of the rear portion of squall lines with trailing stratiform regions in the tropics and midlatitudes and is characterized by "onion-shaped" soundings there (Zipser 1977; Ogura and Liou 1980; Leary and Rappaport 1987). Air near the surface remains cool and moist and is capped by warm, dry air aloft—a condition which, in the tropics, has been observed to suppress future convection for up to 9 to 12 h. The warmest and driest air is typically found at about 1 km AGL and is centered just behind the back portion of the trailing stratiform precipitation region (Zipser 1977; Johnson and Nicholls 1983; Gamache and Houze 1985).

While it is now agreed that subsidence is the primary cause of the wake low, the mechanism for this subsidence has not been firmly established. Brown (1979) has shown that mesoscale downdrafts driven, in part, by precipitation evaporation can lead to adiabatic warming that exceeds evaporative cooling at low levels beneath the stratiform clouds. Miller and Betts (1977) argue that the subsidence in this region is dynamically forced by spreading cool air at the surface. The existence of descending, rear-inflow jets in squall lines may offer yet another explanation for the wake low; however, the cause of these jets is still a matter of speculation. Smull and Houze (1987b) suggest that the rear inflow may be a consequence of two separate processes that generate low pressure areas within the cloud region: (i) hydrostatic reduction of pressure in the lower troposphere behind the leading convective line due to warming aloft in the rearward-sloping deep towers (LeMone 1983) and (ii) hydrostatic lowering of pressure in the midtroposphere in the trailing stratiform region due to latent heating above melting and evaporative cooling (Brown 1979). There is growing evidence to indicate that the midlevel mesolow [in item (ii) above] is a feature separate and distinct from the wake low; however, the relationship between the two mesolows is not well understood. In this paper, it is not our purpose to determine the cause of the rear-inflow jet, rather we will explore its association with the wake low and

[3] Williams notes that descent of warm air all the way to the surface is not common: those areas where it does occur may experience "heat bursts" (Johnson 1983).

determine the relationship of these features to the precipitation structure of the squall line.

3. Data and analysis procedures

The OK PRE-STORM was uniquely designed to investigate the internal and near-environment structure of midlatitude, summertime mesoscale convective systems (MCSs). Numerous convective events occurred during the experiment, with a particularly intense squall passing through the network on 10–11 June 1985 (Cunning 1986; Augustine and Zipser 1987). An overview describing the observational system which captured this squall line can be found in Cunning (1986).

a. Surface mesonetwork and upper air observations

During May and June 1985, an 80-station surface mesonetwork on a 50 km grid was established and operated over Kansas and Oklahoma as one component of OK PRE-STORM (Fig. 2). The northernmost 40 stations consisted of NCAR Portable Automated Mesonetwork (PAM II) instruments. In addition, two PAM II stations were colocated with two stations (S29 and S38) in a 40-station NSSL Surface Automated Mesonetwork (SAM) which made up the southern portion of the surface array. These systems provided 5-minute averages of wind, temperature, wet bulb temperature and pressure; 5-minute maximum wind gusts and 5-minute accumulated rainfall.

The pressure perturbations associated with squall lines can often be quite small (1–3 mb) and the reliability of the analyses depends upon the accuracy of the pressure measurements. The PAM II pressure data,

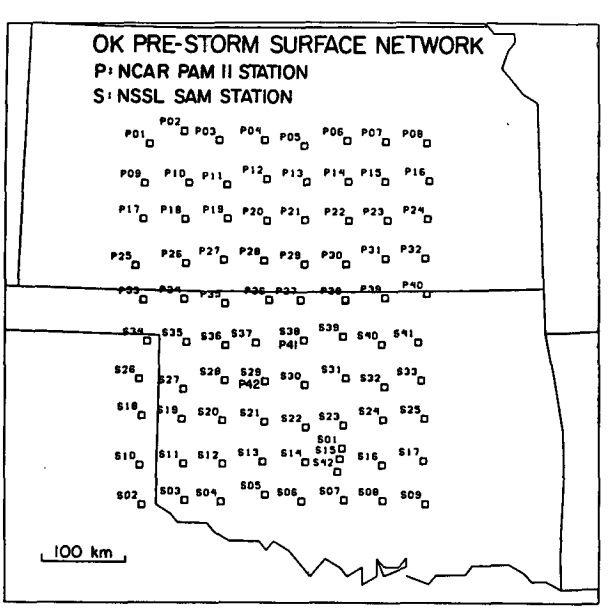

FIG. 2. Oklahoma-Kansas PRE-STORM surface mesonetwork. P and S refer to PAM and SAM stations, respectively.

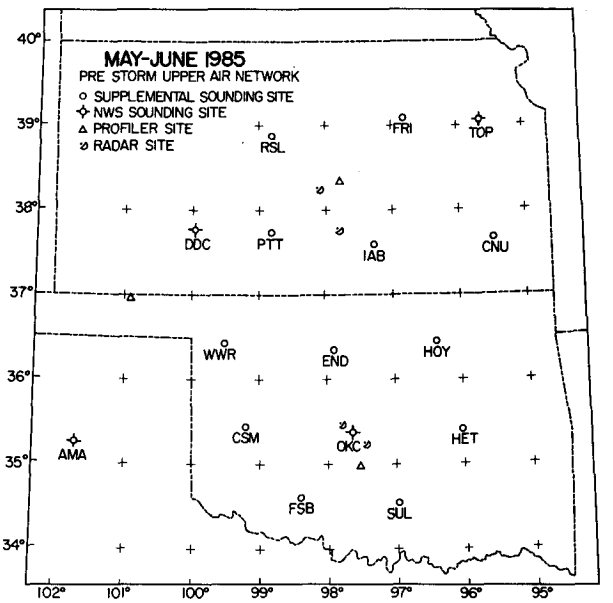

FIG. 3. Oklahoma–Kansas PRE-STORM sounding network.

following the filling of the few (~2%) data gaps by linear interpolation, have been corrected for instrument and elevation errors by consulting calibration records, constructing monthly mean maps and comparing data with National Weather Service (NWS) stations (see the Appendix). The corrected pressure data have an estimated accuracy of 0.3–0.5 mb. The SAM data are not amenable to the same correction procedures as the PAM data due to considerable periods of missing observations. Therefore, procedures described by Fujita (1963) involving analyses and intercomparison of mesonet data with surrounding NWS stations during an undisturbed period just prior to the squall line event have been used to determine corrections to SAM data. Atmospheric tidal effects have been removed using an average of the monthly mean diurnal pressure curves for the NWS stations in the network. These modifications over the period of the analysis range from +1.3 to −0.4 mb. To represent the surface pressure field in our analyses, we have adjusted pressures to 518 m (the average elevation of the PAM II stations)[4] using the surface virtual temperature at each station.

The upper air network consisted of 14 NWS stations (four shown in Fig. 3), 12 supplemental sounding sites and three wind-profiling systems (Cunning 1986). During the passage of the 10–11 June squall line, 90-minute soundings were obtained from the majority of the stations in the network.

A major focus of this paper is on the wake low, which

[4] Our initial analyses (when only PAM data were available) were adjusted to this level, which is sufficiently close to the average elevation of all stations, 480 m, that reanalysis was deemed not necessary, particularly since our primary interest is in pressure gradients.

is best defined during the mature-to-dissipating stage of the squall line (Fujita 1955, 1963; Pedgley 1962; Williams 1963). Although the squall line was never truly in steady state (to be shown later), we have chosen to prepare composite analyses of sounding data over a relatively short 3-h period during the latter stage of the squall line lifetime (12–15 h duration) in order to provide a detailed analysis of the wake structure. Our procedure in preparing composite horizontal maps of the fields has been to displace soundings forward and backward in space (or time) from a central time of 0600 UTC (all times are UTC), 11 June, using translation directions and speeds determined from gust front (wind shift) isochrones (Fig. 4). Interpretations of the composite will have to be tempered by consideration of the nonsteadiness of the line; however, this limitation is felt not to be severe for the short 3-h period of the composite during a portion of the mature-to-dissipating stage of the squall lifetime. Horizontal balloon displacements have been included in all analyses.

Where appropriate, data from the three wind profiling systems (Fig. 3; also see Augustine and Zipser 1987, for detailed discussion of profiler data for this case) have been utilized in the analyses.

b. Radar and satellite data

Since in this study we are interested in the broadscale aspects of the surface pressure field associated with this very long squall line, we have used data from the NWS surveillance (WSR-57) radars in Wichita, Kansas; Oklahoma City, Oklahoma and Amarillo, Texas. Base scan (0.5° elevation angle) data, giving the low-level reflectivity field, are displayed in our analyses.

Satellite data are from GOES West, a U.S. geostationary satellite, situated at 105°W during the experiment.

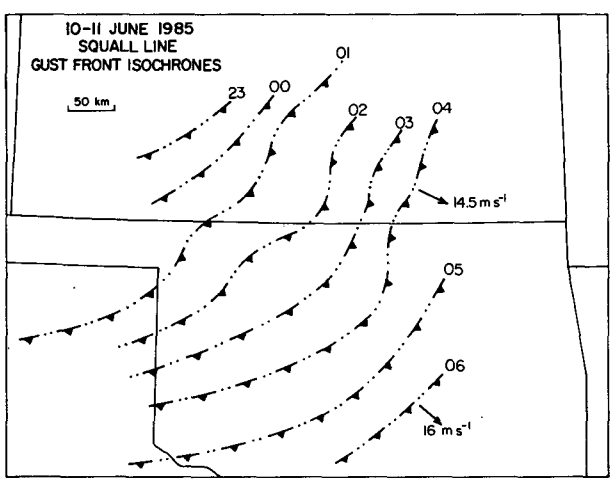

FIG. 4. Squall-line gust front isochrones for 10–11 June 1985, determined from surface mesonetwork data. Extensions outside mesonetwork area are estimated from radar data.

4. Synoptic overview

A sequence of regional surface analyses depicting a portion of the life history of the squall line is shown in Fig. 5. A cold front is entering the western portion of the region at 2100 (Fig. 5a) with the remnant of a decaying mesoscale convective system (MCS) evident over eastern Kansas. Visible satellite imagery at this time (Fig. 6) shows the decaying MCS, as well as the developing squall line. The initial cells in the squall line appear to be forming ahead of the surface cold front in a broken areal-type development (using the definition of Bluestein and Jain 1985), although the exact position relative to the front is difficult to determine.

The most significant thunderstorm in Kansas during the formative stage of the line occurred near Garden City (Fig. 7; just outside the PAM mesonet area) around 2200 (marked A in Fig. 6a). Significant weather associated with this system included 2 to 3 cm hail and wind gusts to 31 m s^{-1}. Strong surface cooling was reported at Garden City, Dodge City and the stations in the southwestern portion of the PAM mesonet with the passage of this storm. The thunderstorm track also coincided reasonably well with the track of the most intense mesohigh along the squall line (Fig. 7), a feature that will be evident from later analyses. Apparently, this hail-bearing storm (the only reported one in Kansas associated with the squall line) produced a significant cold dome and mesohigh that may have modified slowly enough to contribute to an asymmetrical structure of the surface pressure field in the mature squall line.

The squall line intensified, expanded and moved to the southeast by 0000 (Figs. 5b and 6b). Near the Kansas–Oklahoma border, the squall line gust front intersected a weak outflow boundary from the preexisting MCS in eastern Kansas. This boundary had propagated to the southwest from 2100 to 0000 (cf. first two panels in Fig. 5; mesonet data have been used to define its position). A tornadic thunderstorm formed at the intersection of these boundaries (tornado at Ashland, Kansas, at 0017; Fig. 7) perhaps triggered by the boundary intersection mechanism described by Purdom (1976). A sounding from Pratt, Kansas (see Fig. 7 for position) at 2330 on the 10th (Fig. 8) shows pronounced convective instability and strong clockwise turning of the low-level shear vector (Fig. 8 insert), a condition favorable for tornadic storms (Maddox 1976; Klemp and Wilhelmson 1978).

The convective available potential energy (CAPE; Moncrieff and Miller 1976; Weisman and Klemp 1982) and bulk Richardson number (Ri; Moncrieff and Green 1972; Weisman and Klemp 1982) for the Pratt sounding are 2300 m^2 s^{-2} and 25 (computed using expressions in Bluestein and Jain 1985). This value of CAPE agrees rather well with the mean of 2120 m^2 s^{-2} for eight broken areal cases reported by Bluestein and Jain, but

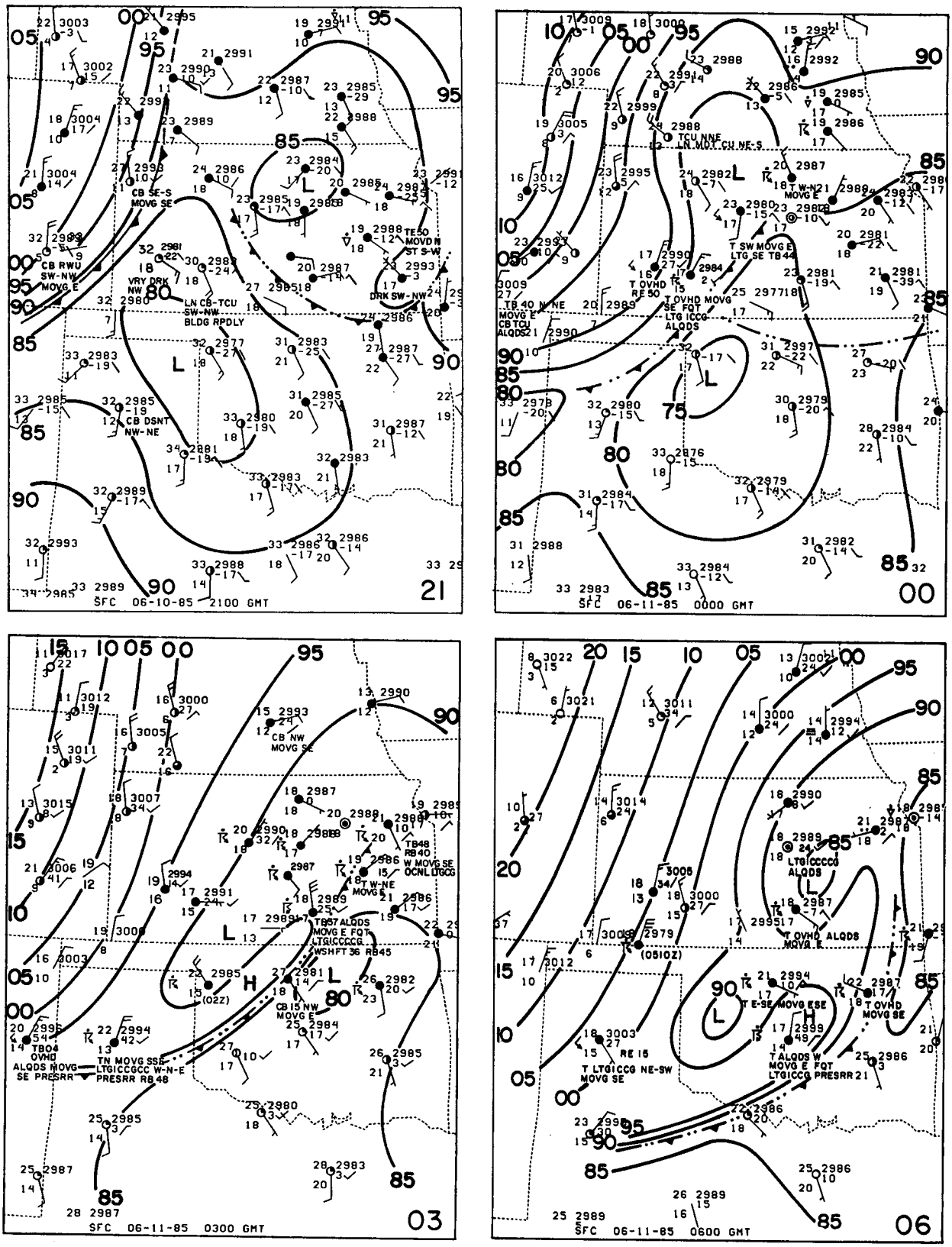

FIG. 5. Surface mesoanalyses at 21, 00, 03 and 06 UTC depicting squall line passage. Some features are drawn with the aid of surface mesonetwork data illustrated later. Dashed double-dot lines are gust fronts or outflow boundaries. Isobars are drawn for altimeter settings: units are in Hg, e.g., 85 = 29.85 in Hg. For wind speed, one full barb = 5 m s^{-1}, one half barb = 2.5 m s^{-1} (similarly in subsequent figures).

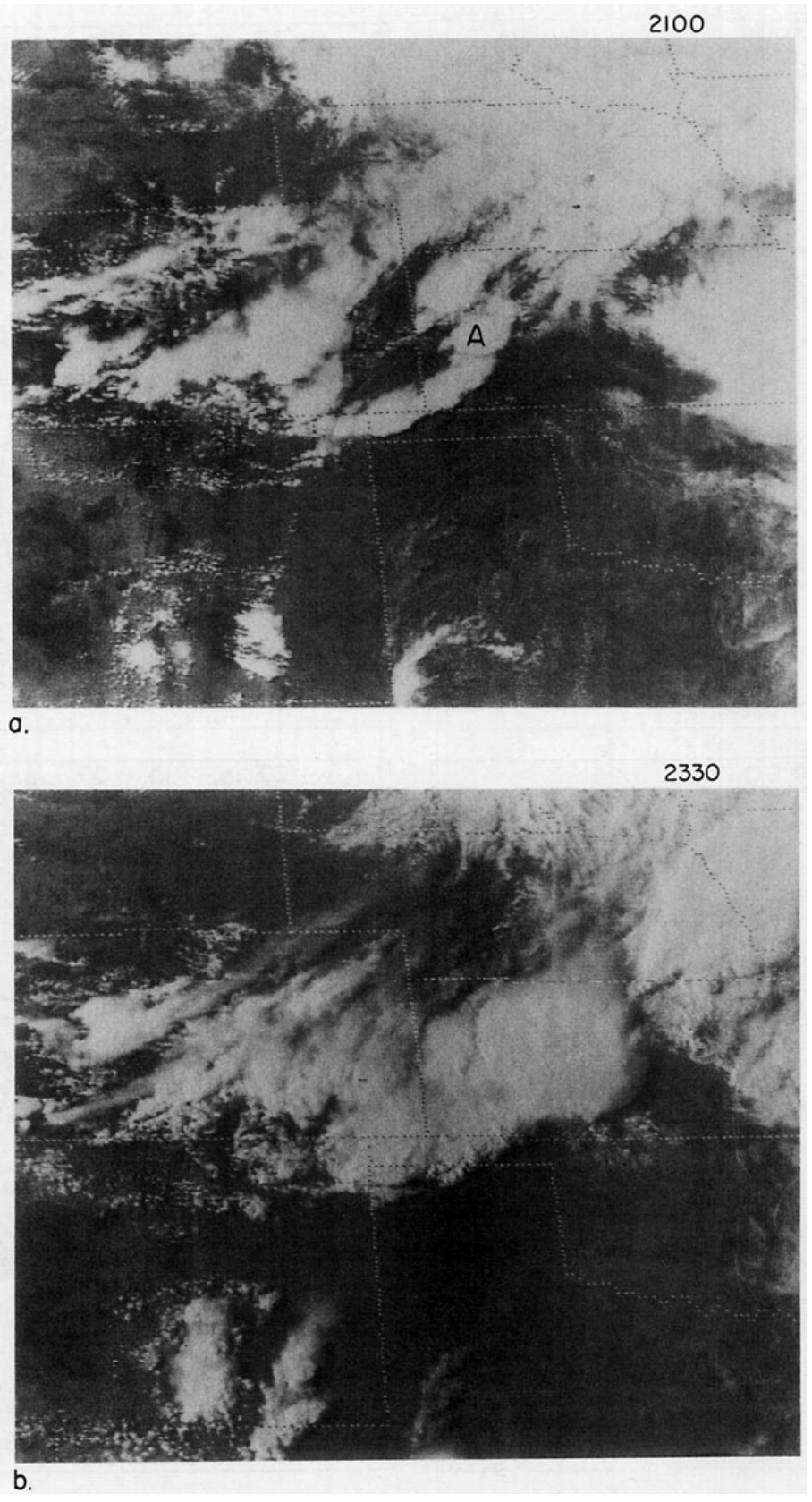

FIG. 6. Visible satellite images at 2100 (a) and 2330 UTC (b). Intense cell affecting Garden City, Kansas area marked by A.

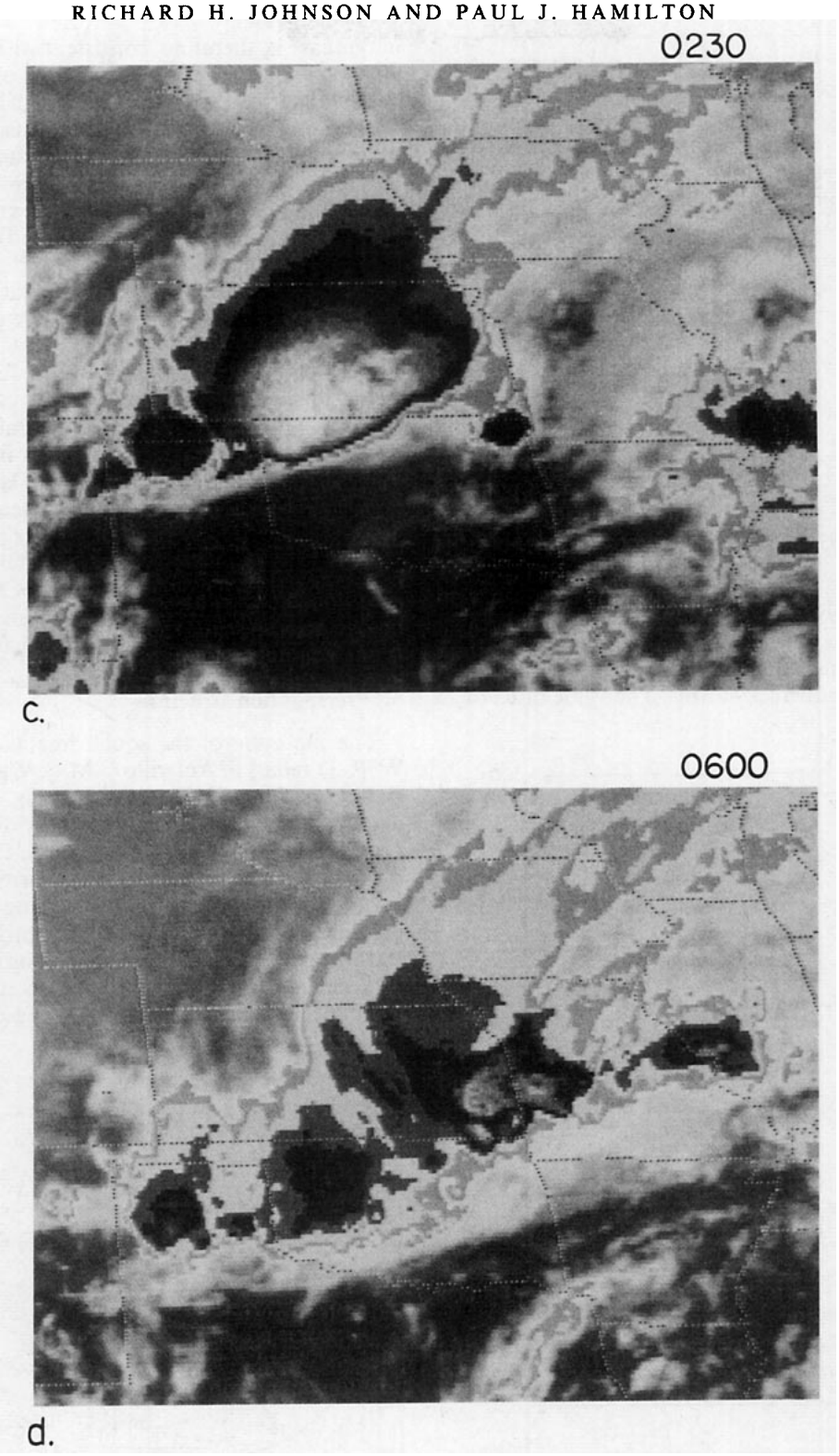

FIG. 6. (*Continued*) Infrared satellite images at 0230 (c) and 0600 UTC (d).

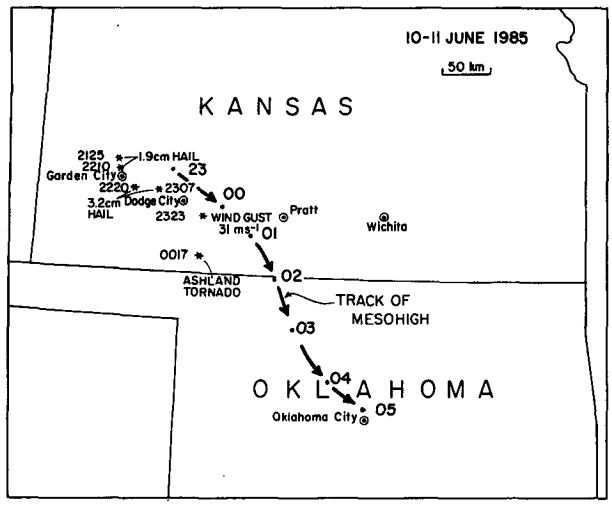

FIG. 7. Severe weather in southwestern Kansas during formative stage of squall line. Subsequent track of mesohigh is indicated.

Ri is considerably smaller than their broken-areal mean of 56. Weisman and Klemp (1982) have shown from observational and numerical studies that $15 \leq \mathrm{Ri} \leq 35$ is indicative of supercell storms. The value of Ri of 25 in our case is, therefore, consistent with the fact that a tornado was observed in the vicinity of Pratt.

By 0300 (Figs. 5c and 6c), the squall line moved into Oklahoma and was near its peak intensity with a length of over 500 km. Altimeter setting data from the conventional NWS surface stations show some evidence of a pre-squall mesolow, a mesohigh and a weak wake low. Finally, at 0600 (Figs. 5d and 6d) the squall line was well into its dissipating stage, and a mesohigh and two wake lows are evident (these features are drawn with the aid of mesonetwork pressure data to be illustrated later).

The 500 mb flow at 0000 UTC 11 June is presented in Fig. 9. A significant short-wave trough, moving east at 16 m s^{-1}, is evident over the central United States. This trough, which probably had an important influence on the squall line development, later contributed to (perhaps assisted by latent heat release in the squall line itself) surface cyclogenesis farther to the east, with a low tracking from Missouri to the Ohio Valley. The winds at two locations in Kansas (DDC and TOP) have been influenced by the squall line and reveal a substantial departure from geostrophic balance.

5. Precipitation structure

The life cycle of the squall line as viewed by the WSR-57 radars in Amarillo (AMA), Wichita (ICT) and Oklahoma City (OKC) is shown in Fig. 10. Reflectivity data from the base scans of the individual radars have been merged to form the composites. Early on (2300–0100), the primary precipitation occurred in the leading convective line with only weak trailing stratiform rain present. The thunderstorm which produced the tornado near the Oklahoma–Kansas border at 0017 can be seen ahead of the squall line in the 0000 panel. During the period 0200 to 0400 the convective line

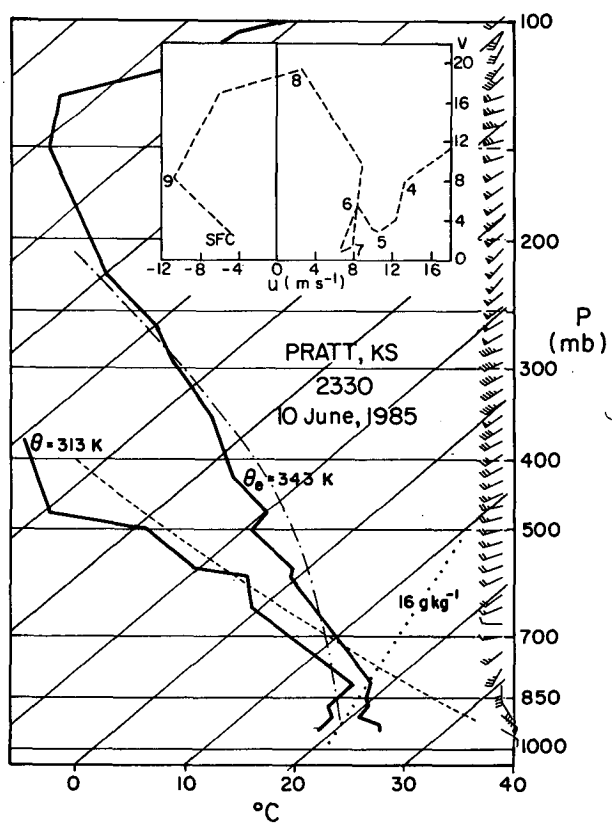

FIG. 8. Skew-T diagram of sounding from Pratt, Kansas, at 2330 UTC. Inset shows hodograph with 9, 8, . . . indicating 900, 800, . . . mb.

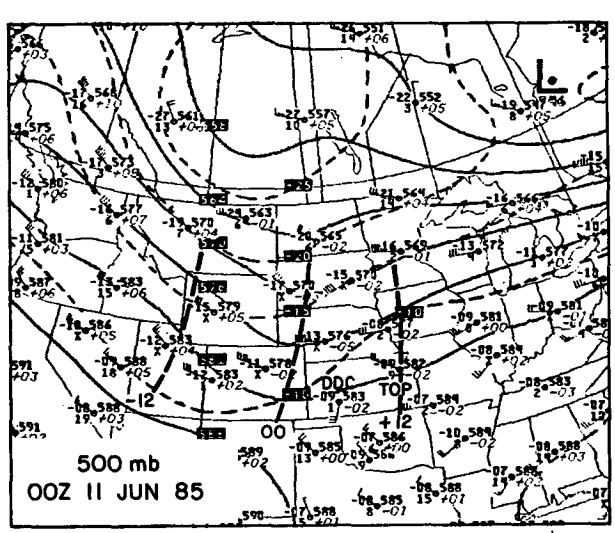

FIG. 9. 500 mb analysis at 0000 UTC 11 June 1985. Heavy dashed lines mark 12-h previous, current and 12-h later trough positions.

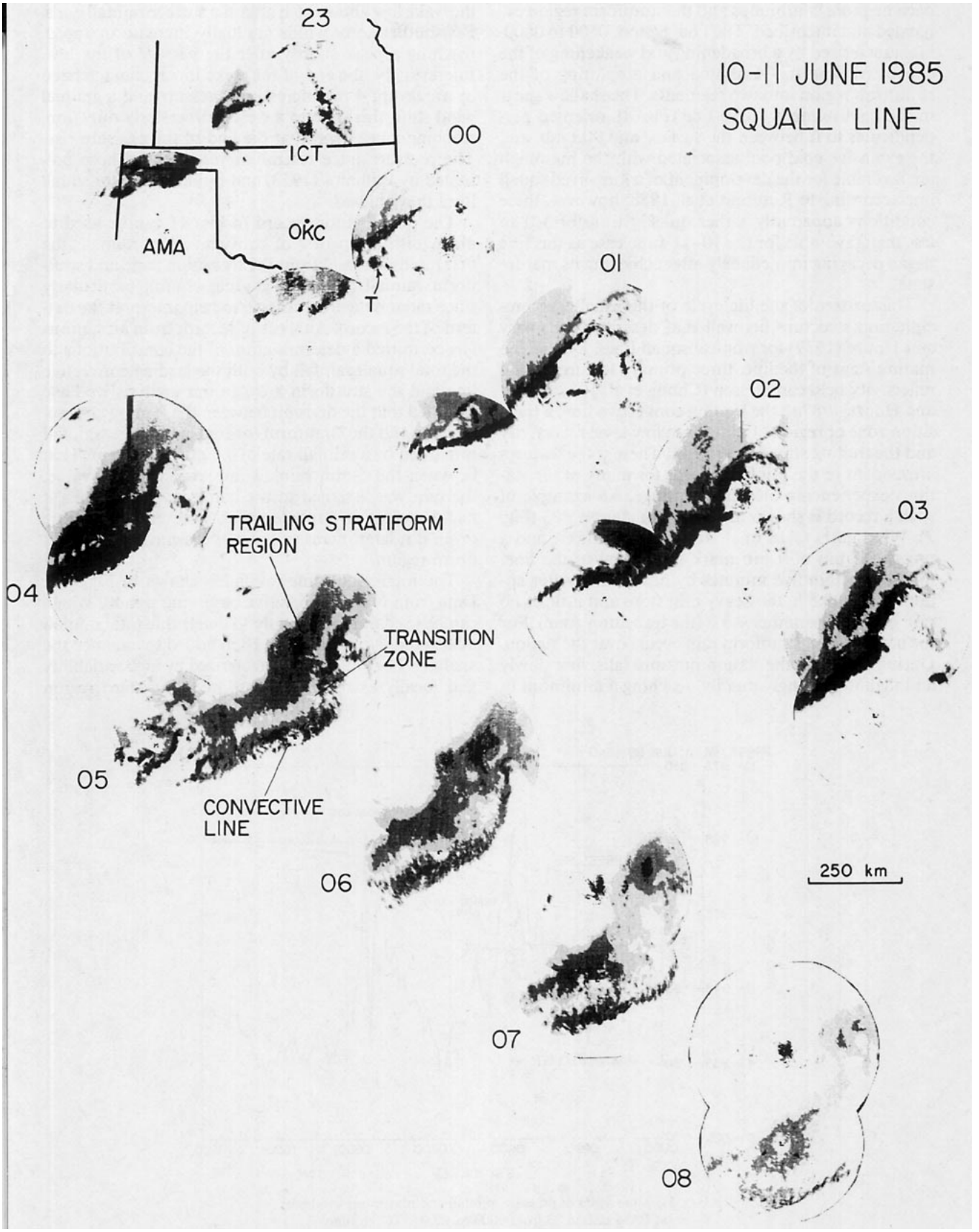

FIG. 10. Hourly sequence of merged NWS WSR-57 base scans from Amarillo (AMA), Wichita (ICT) and Oklahoma City (OKC) radars (2300 to 0800 UTC). Reflectivity thresholds are 15, 25, 35 and 50 dBZ. T in 00 panel refers to tornado-bearing thunderstorm.

became more continuous and the stratiform region expanded and intensified. The final period, 0500 to 0800, is characterized by a broadening and weakening of the convective line in Oklahoma and a splitting of the stratiform region into two segments. The shallow shear in the environment of the line (Fig. 8), oriented perpendicular to it between the surface and 900 mb, and the extensive cold pool associated with the mesohigh are favorable for the development of a long-lived squall line according to Rotunno et al. 1988; however, these conditions apparently rather quickly transformed to less than favorable for the 10–11 June case as this line began decaying immediately after achieving its mature state.

This pattern of the life cycle of the squall line precipitation structure fits well that described by Leary and Houze (1979) for tropical squall lines. During the mature stage of the line, three primary features in the reflectivity field can be seen (Chong et al. 1987; Smull and Houze 1987a): the leading convective line, a transition zone or region of minimum low-level reflectivity and the trailing stratiform region. These three features are evident in the rainfall records for many of the stations experiencing the squall passage. An example of such a record is shown in Fig. 11 for station P23 (Fig. 2). Wind gusts to 18 m s^{-1} from the northwest and a pressure jump of 4 mb mark the arrival of the line, followed within five minutes by heavy rain. After approximately 0.5 h, the heavy rain stops and little to no rain occurs for another 0.5 h (the transition zone). For the next 2 h light stratiform rain occurs over the station. During this time, the station pressure falls, first slowly and then increasingly rapidly, reaching a minimum in the wake low about 0.5 h after the surface rainfall ends. Eastsoutheasterly winds gradually increase in speed, reaching a peak shortly after the passage of the low. Interestingly, the end of the wake low is characterized by an abrupt 4 mb increase in pressure and a gradual wind shift, this time to a westnorthwesterly direction, reaching a peak speed at the end of the pressure rise. The pressure trace resembles very closely those presented by Williams (1953) and Fujita (1955) for squall lines they studied.

The precipitation record in Fig. 11 can be used to distinguish the period of convective line rainfall (the first rapid increase) from the transition zone and stratiform rainfall (the later gradual climb), particularly since radar data are available to help interpret the pattern of the record. Analysis of records from all stations has permitted a determination of the contributions to the total squall rainfall by both the leading convective line and the stratiform area. In our analysis we have assumed that the division between the leading convective line and the stratiform (or transition zone) rainfall is marked by a rainfall rate of 0.5 mm per 5 min. That is, when the 5-min rainfall rate exceeded this value, the rain was assigned to the convective line; when it had decreased to a rate less than or equal to this value (even if it later increased), it was assigned to the stratiform region.

The total squall line rainfall is shown in Fig. 12a. Data from NWS cooperative observing stations which can be used unambiguously to determine total rainfall due to the squall line have been added to enhance the analysis. The pattern is characterized by high variability and locally extreme amounts in the western region

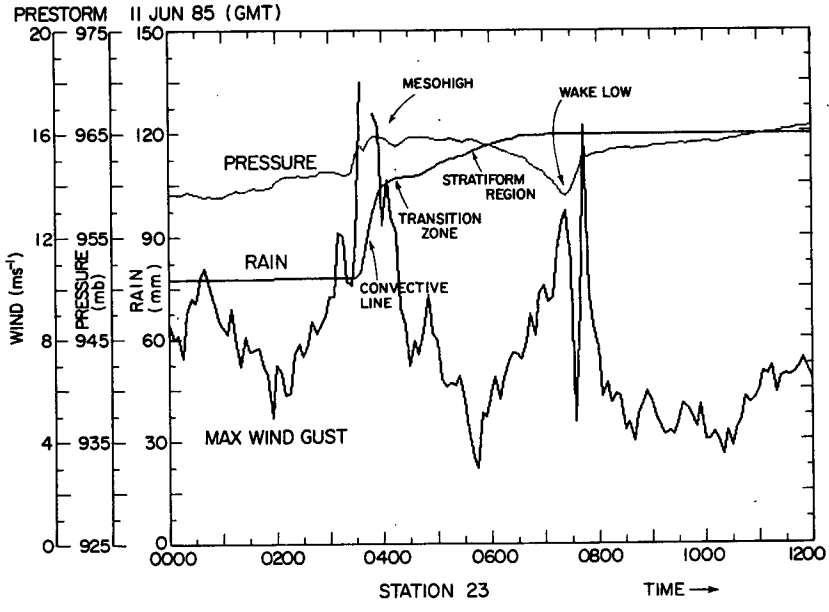

FIG. 11. Time series of pressure, rainfall and maximum wind gust at PAM station 23 from 0000 to 1200 UTC 11 June.

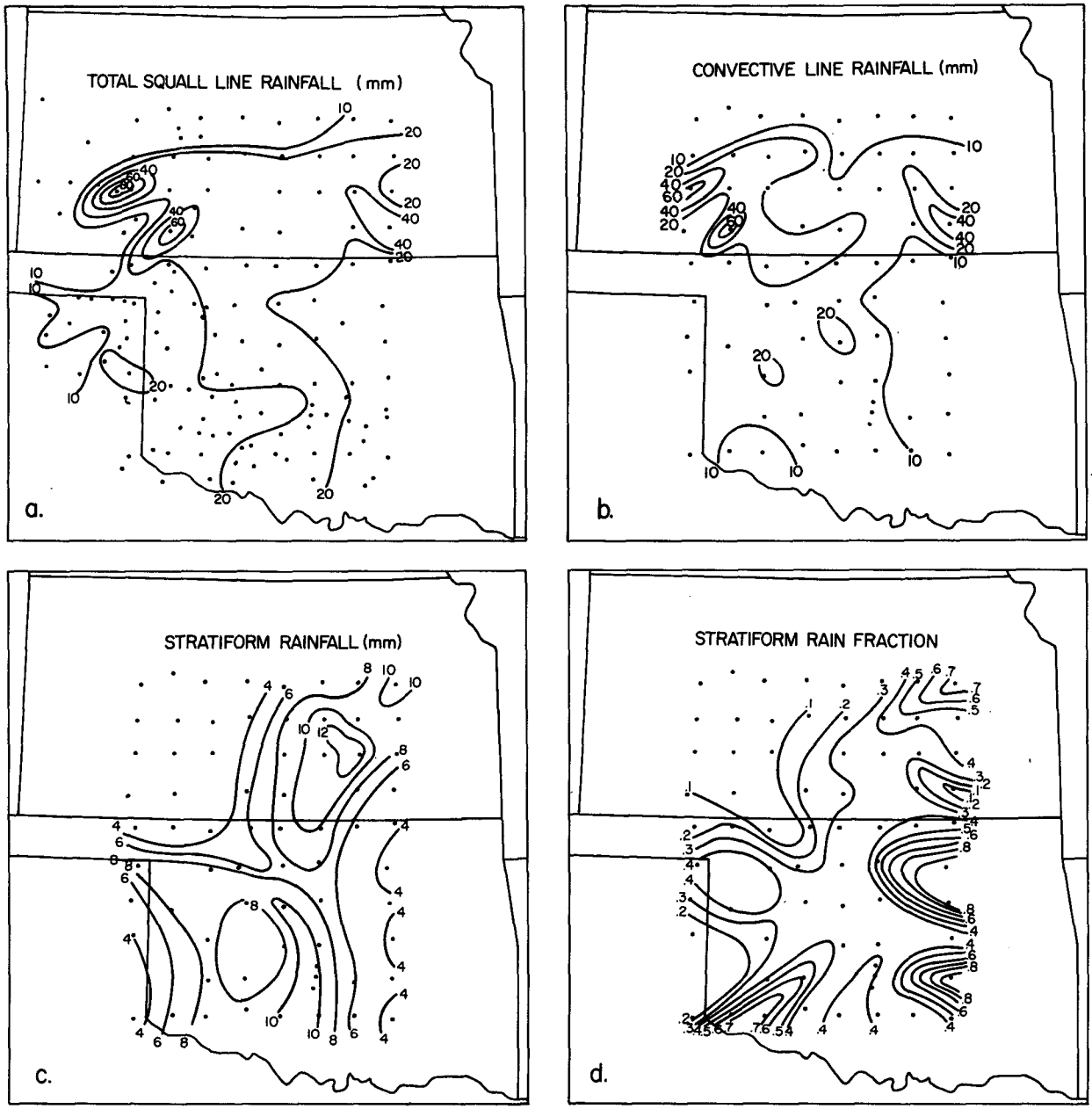

FIG. 12. Rainfall from entire squall line (a), leading convective line (b), stratiform component (c) and fraction of total squall line rainfall due to stratiform component (d). Station data used in the analysis indicated by dots.

(initiation phase), comparatively uniform amounts (20–30 mm) in the central portion (mature phase) and a return to large variability in the east (dissipating phase). The convective line component (Fig. 12b) has a pattern similar to the total rainfall, except that amounts diminish significantly over much of the eastern portion of the network where the convective line weakens (Fig. 10). The stratiform rainfall estimated from the precipitation records is shown in Fig. 12c. The maximum precipitation from the stratiform cloud system occurs in the east-central portion of the network. This distribution is consistent with the radar reflectivity life cycle (Fig. 10) which shows a maturation of the stratiform region in this portion of the network. Two separate maxima exceeding 10 mm are observed corresponding to the split stratiform reflectivity maxima in Fig. 10. Since the line was moving to the southeast at 15 m s^{-1}, it is apparent that the stratiform precipitation region did not ever reach steady-state intensity.

The fraction of the total squall line rainfall from the stratiform component (Fig. 12d) generally increases from west to east although there is considerable vari-

ability in the southern and eastern part of the network. During the mature stage of the squall line, approximately 30 to 40% of the total rainfall can be attributed to the stratiform area. The average fraction for the portion of the mesonet traversed by the squall line (virtually all stations except for several in the northernmost row) is 29%. This fraction for the entire area and lifetime of the squall line cannot be determined from the surface raingage measurements, despite the existence of an expansive surface mesonetwork in OK PRE-STORM, due to the immense size of the storm system. Nevertheless, a sufficient fraction of the squall line was sampled to conclude that the stratiform fractional contribution to the total rainfall for this midlatitude squall line is comparable to the approximately 30 to 40% determined from radar data for tropical squall lines observed during the GARP Atlantic Tropical Experiment (GATE) and the Winter Monsoon Experiment (Houze 1977; Cheng and Houze 1979; Gamache and Houze 1983; Houze and Rappaport 1984; Leary 1984; Churchill and Houze 1984; Wei and Houze 1987).

6. Surface pressure features

We next examine the field of surface pressure during the passage of the squall line over the mesonetwork. The first analysis (2300, Fig. 13a) shows the formation of a mesohigh in the western portion of the network in an area near the Garden City severe storms (Fig. 7). Additionally, there is a mesohigh–wake low couplet in east-central Kansas and a decaying outflow boundary on its southern edge associated with the dissipating MCS in that area. No wake low to the rear of the approaching squall line is yet evident in this initiation stage (cf. Fig. 1). By 0100 (Fig. 13b) the squall mesohigh has intensified, expanded and moved to the southeast. A weak pre-squall mesolow can be seen, as well as a further weakened high–low couplet from the preexisting MCS. A bulge or bowing of the squall line exists where the old outflow boundary intersects the gust front. This feature is also coincident with the mesohigh and marks the location where the pre-squall tornadic thunderstorm (0000 and 0100 panels in Fig. 10) was incorporated into the line. Light, stratiform precipitation is beginning to develop and expand behind the line and there is a slight hint of a wake low forming.

Although barely discernible at 0100, the wake low rapidly becomes well defined by 0130 (not shown) and at 0300 (Fig. 13c) it is a very extensive feature positioned at the back edge of the stratiform precipitation region. The axis of the wake low is roughly aligned along the 0300 surface rainfall termination isochrone (determined from the 5 min mesonet data). Importantly, this 0100–0300 period coincides with a rapid intensification of the stratiform precipitation region. A single pre-squall mesolow can also be seen at this time.

At 0500 (Fig. 13d) the stratiform region has expanded dramatically and further intensified (also evident in the rainfall analysis in Fig. 12c). The wake low has now split into two parts while the mesohigh continues as a single entity propagating toward the southeast maintaining about the same amplitude. The wake low continues to "hug" the back edge of the stratiform area and align itself along the rain termination isochrone. The 0700 analysis (Fig. 13e) shows a continued separation of the wake lows as well as a splitting of the stratiform region into two main segments (also discussed in Rutledge et al. 1988).

This life cycle of the 10–11 June 1985 squall line surface pressure features resembles very closely that described many years ago by Williams (1953, 1963), Fujita (1955, 1963) and Pedgley (1962). It follows Fujita's schematic (Fig. 1a), except for the splitting of the wake low in this case (which may not be common) and the existence of a pre-squall mesolow. A summary of the tracks of the mesohigh and wake low features is presented in Fig. 14. The splitting occurs around 0500 and the tracks of the wake lows and the trailing stratiform reflectivity maxima are divergent thereafter. In cases where a single wake low is observed, the track of the low is slightly to the left of the mesohigh track (Pedgley 1962). The northern wake low–mesohigh couplet in our case corresponds to this situation. The intensities of both wake lows fluctuate somewhat (by several mb) and there is a sharp increase in the pressure gradient at the backside of the Kansas mesolow late in the period (see Figs. 11 and 13e). The mesohigh tracks uniformly and with nearly constant amplitude to the southeast throughout the period and, as discussed in section 3, can be traced back to the severe thunderstorms in southwestern Kansas during the formative stage of the line. Based on this single case study, one might expect that the behavior of mesohighs and wake lows for an individual squall line depends importantly on the evolution of both the leading convective line and stratiform precipitation regions, and asymmetries that occur within them. The evolution of these latter features, in turn, depends on many factors: environmental wind shear, thermodynamic stratification, outflow boundaries, storm life history and others. An explanation for the splitting of the wake low and the stratiform area in the PRE-STORM case is beyond the scope of our study.

A prominent feature of the surface analyses at 0300, 0500 and 0700 (Figs. 13c–e) is surface flow through the wake low with a confluence axis occurring 20–50 km to the rear of the wake low center. This behavior of the surface flow in the wake low area is similar to that illustrated in the many cases presented by Williams (1953), Fujita (1955) and Pedgley (1962), but it is not represented in the schematic of Fujita (Fig. 1, bottom) nor those presented by Pedgley. Our revision of this schematic structure will contain this feature. The sur-

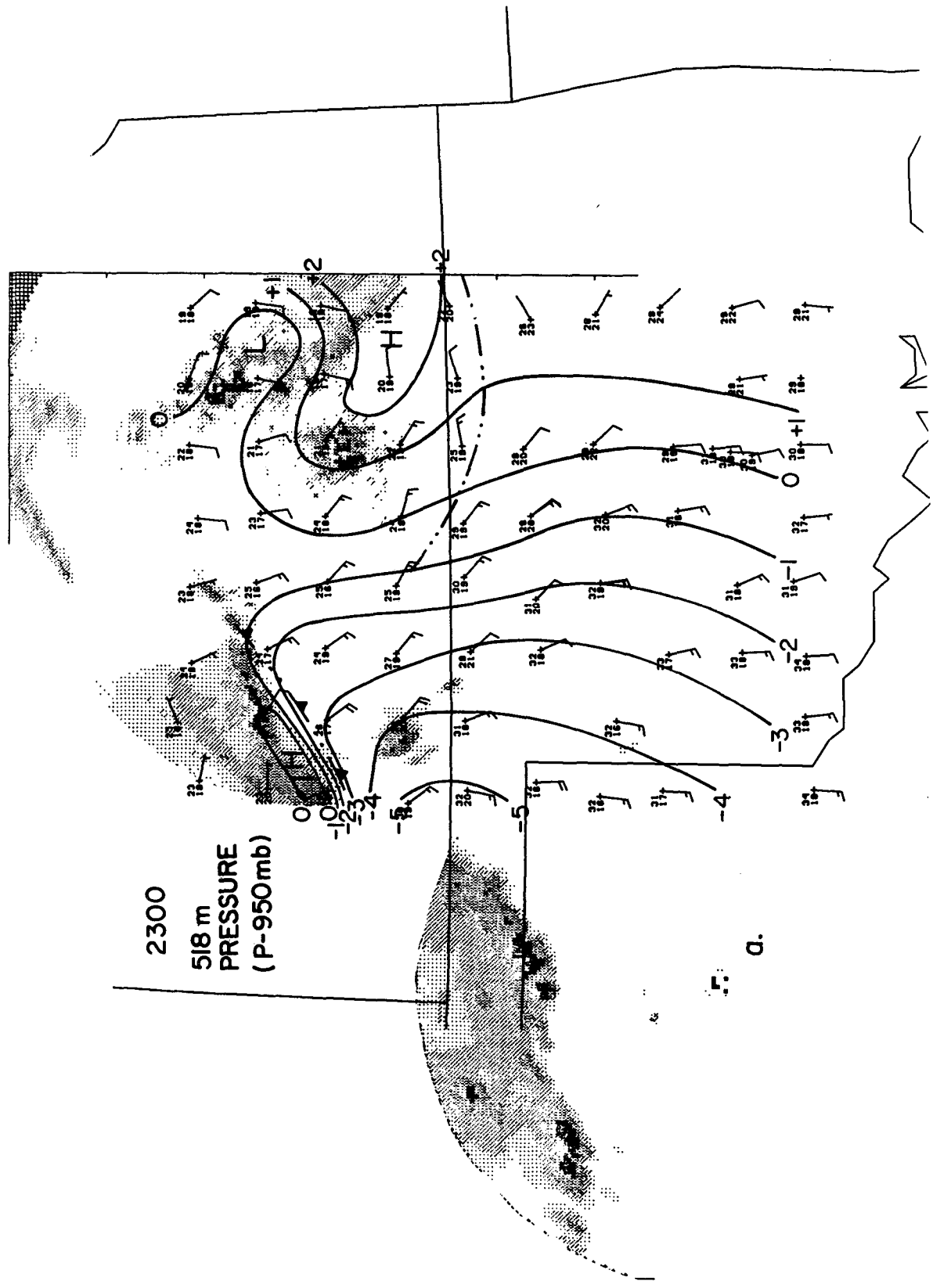

FIG. 13. Pressure at 518 m indicated as departures, in millibars, from 950 mb at 2300 (a), 0100 (b), 0300 (c), 0500 (d) and 0700 (e). Reflectivity thresholds are 15, 25, 35 and 50 dBZ. Dashed double-dot lines are gust fronts or outflow boundaries. Dotted line marks termination of surface rainfall based on surface mesonetwork data. Temperature and dewpoint (°C) are plotted at individual stations.

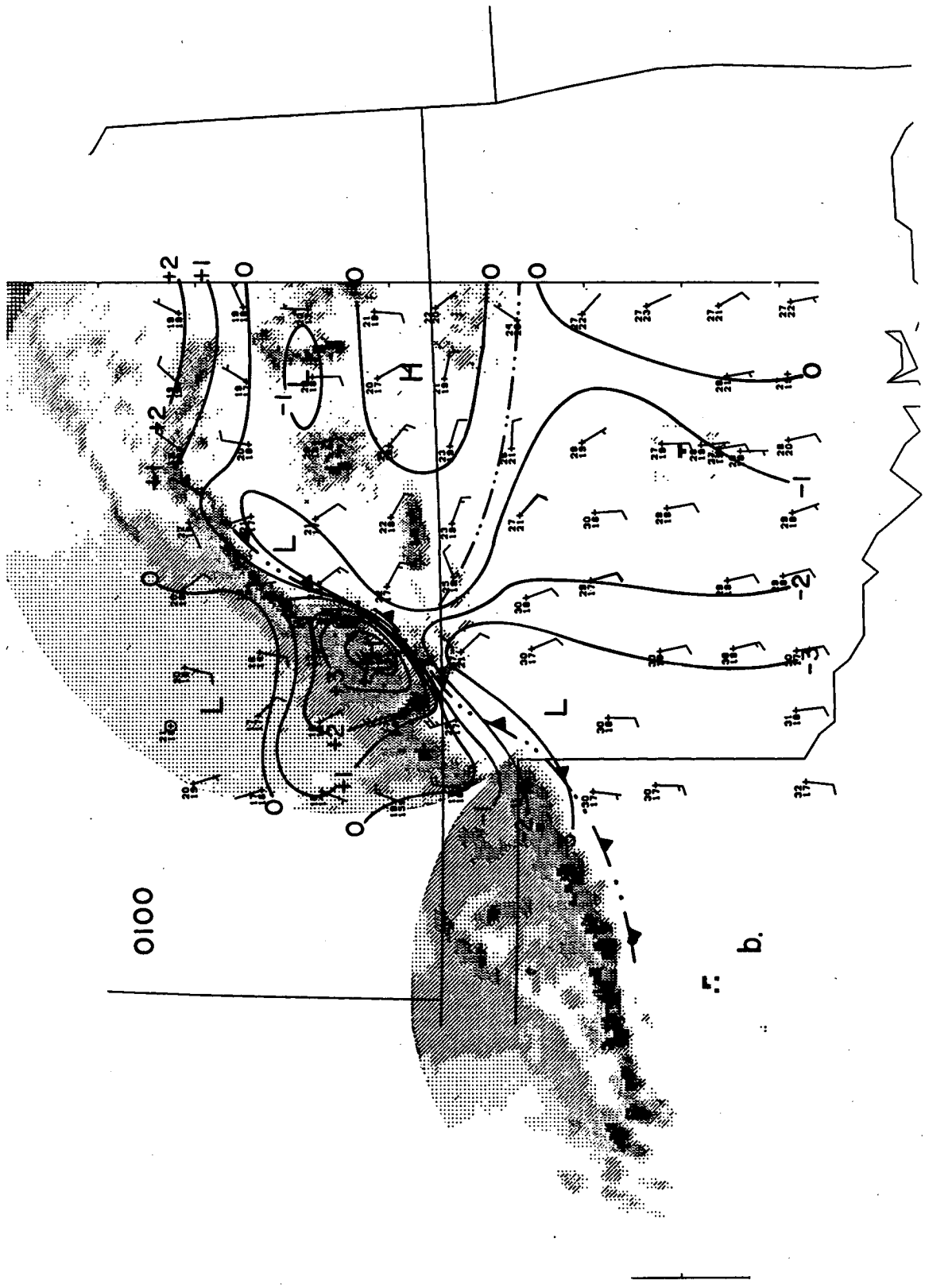

FIG. 13. (*Continued*)

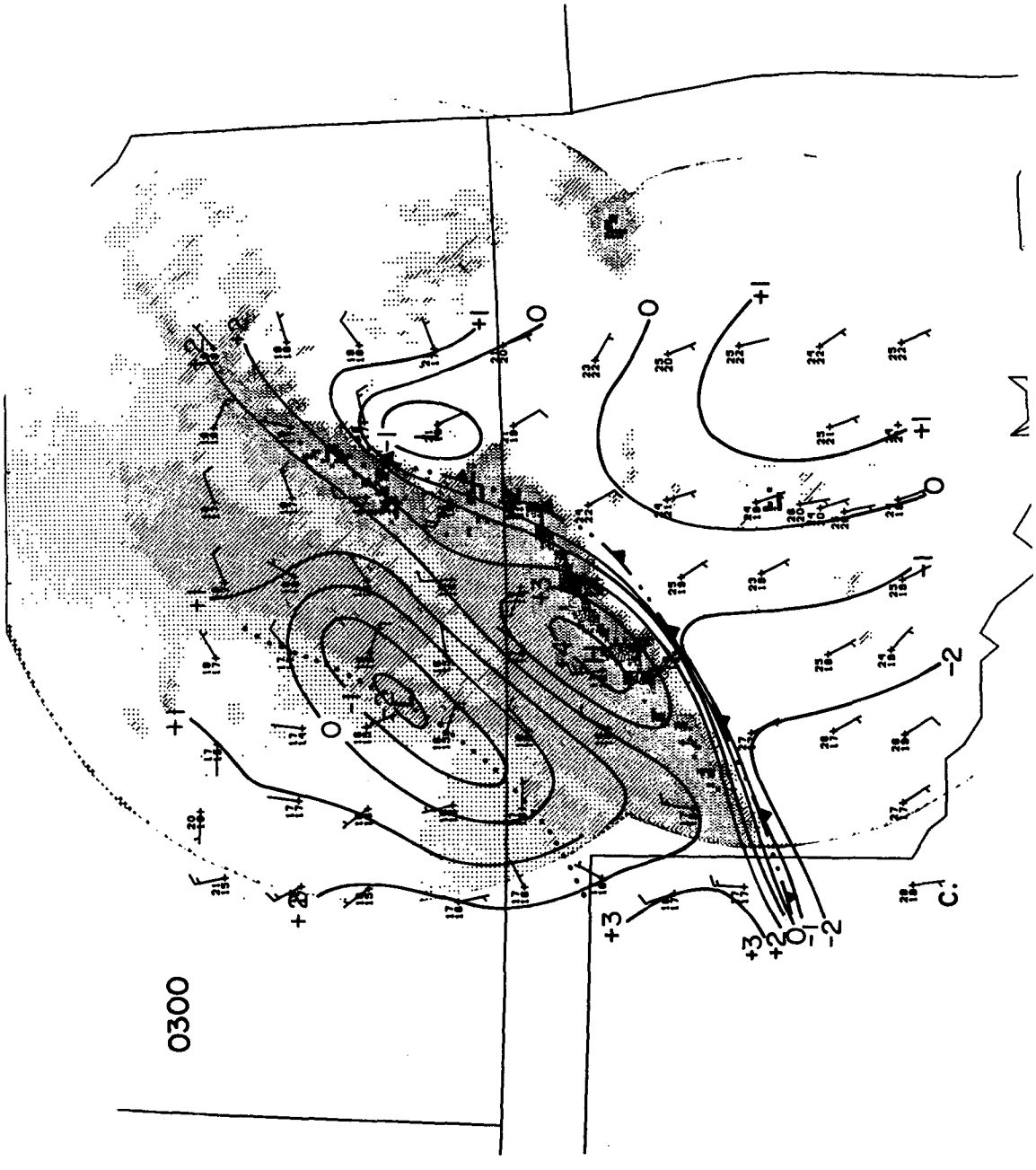

FIG. 13. (*Continued*)

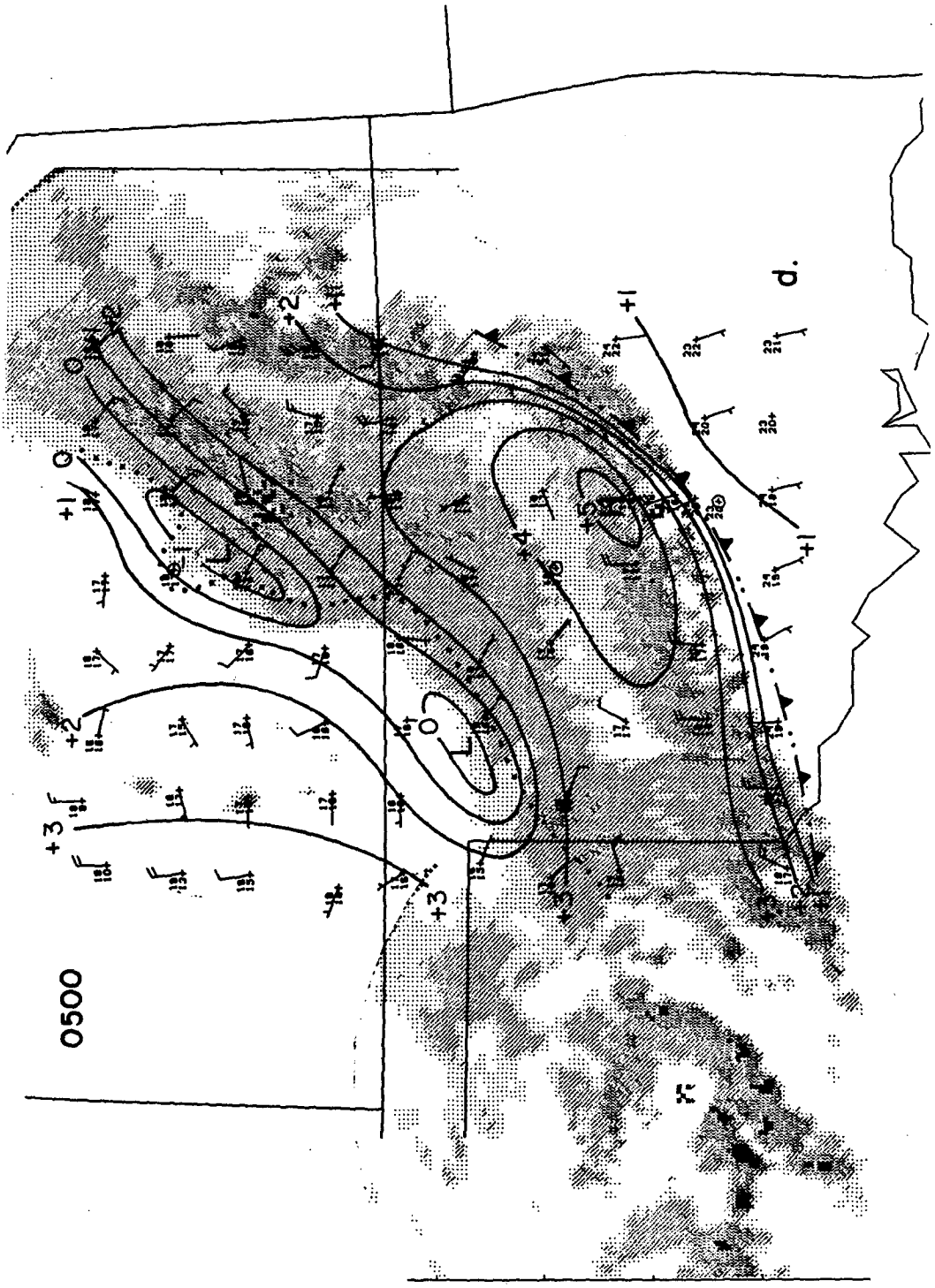

FIG. 13. (*Continued*)

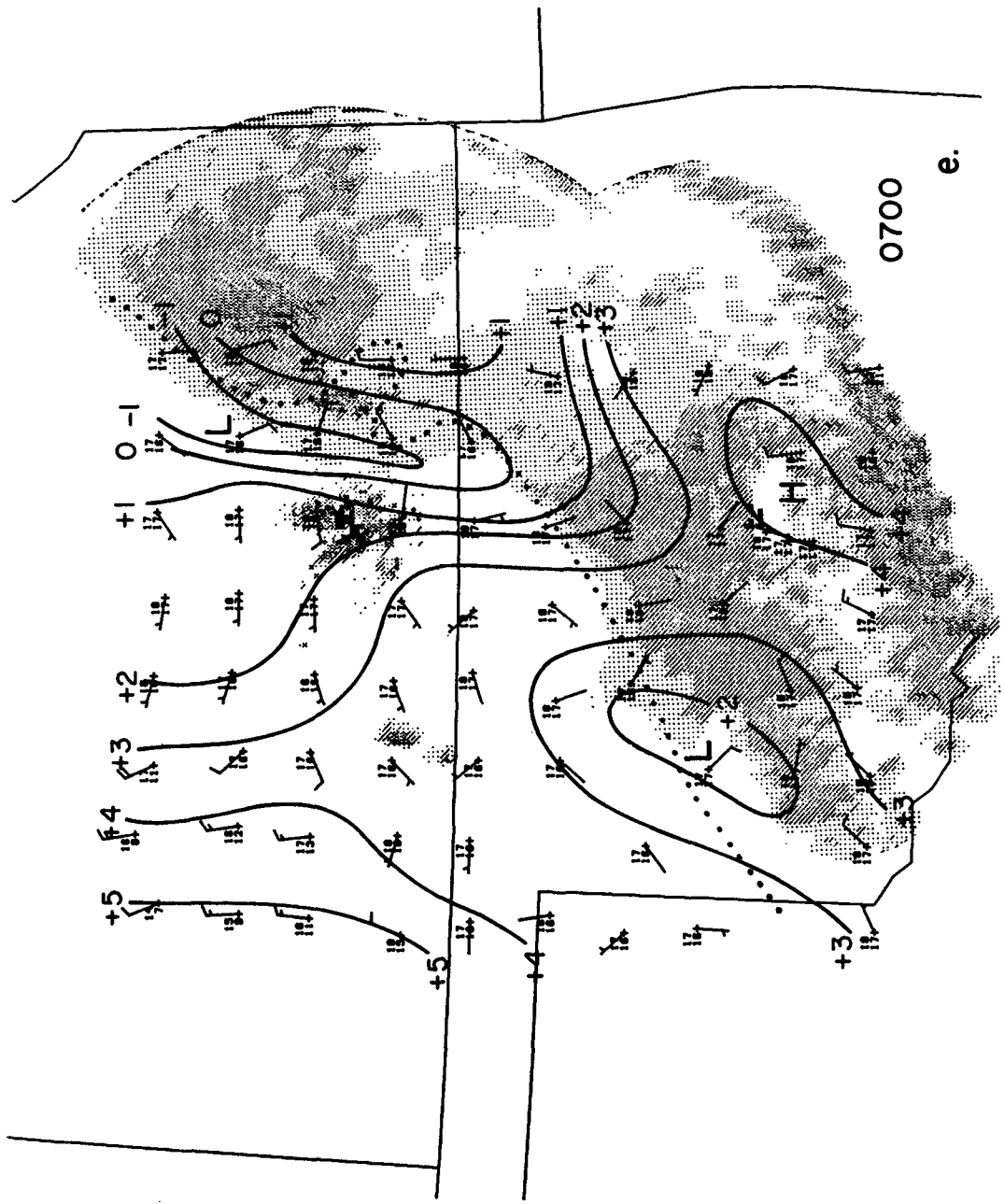

FIG. 13. (*Continued*)

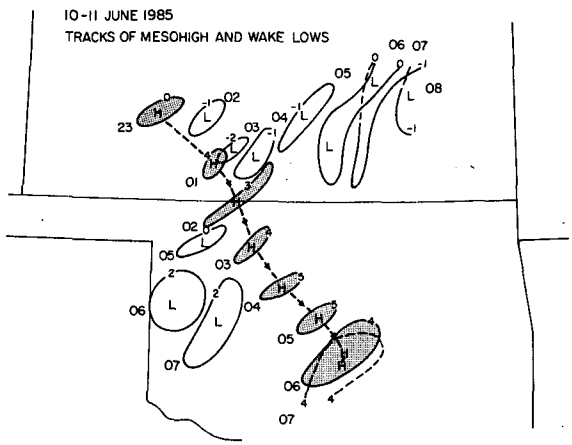

FIG. 14. Tracks of mesohigh and wake lows for 10–11 June 1985 squall line from 2300 to 0800 UTC. Innermost closed isobars are drawn (labels are departures of pressure, in mb, at 518 m from 950 mb).

face convergence to the rear of the wake depression might reasonably be expected to trigger new convection (Williams 1963). Indeed, a line of weak convection formed to the rear of the stratiform precipitation region in this storm, as well as in several other PRE-STORM cases. However, in the 10–11 June case (and presumably others) strong lower-tropospheric subsidence in this region effectively capped the growth of these cells and prevented any deep convection from forming (Koch and McCarthy 1982).

7. Rawinsonde composite analysis (0430–0730 UTC)

Here we present the composite structure of the squall line wake during the mature stage of the wake low for a 3-h period centered at 0600. The wake low was not in steady state during this period (Fig. 14) and, in fact, exhibited splitting; nevertheless, it is argued that the changes are not sufficiently great during this mature stage of the stratiform region to invalidate the analysis for this short interval. A composite at an earlier time (0300) was attempted, but two factors led to difficulties in analysis then: 1) the lack of sufficient soundings in the trailing stratiform region and 2) a greater degree of nonsteadiness as the wake low and stratiform areas were developing rapidly (Figs. 10 and 12).

To obtain a perspective of the flow relative to the squall line in the vicinity of the wake, three cross sections perpendicular to the line have been constructed (positions marked in Fig. 15). Sections AA′ and CC′ transect the two wake lows whereas along BB′ only a weak pressure minimum is present. Several hours earlier (0200 to 0400) a single, intense wake low existed along BB′ (Figs. 13c and 14). This region corresponded to a concavity or "notch" (Smull and Houze 1985) on the back edge of the stratiform area (Figs. 10 and 13c and 13d), a position which Smull and Houze suggest is characterized by the strongest rear inflow into the system. Smull and Houze indicate that this descending inflow current can extend all the way to the surface and meet up with the leading convective line, causing it to bow forward and weaken. Doppler radar data coverage in our case is, unfortunately, insufficient to determine whether or not a similar sequence of events occurred. However, the Doppler radar analysis of Rutledge et al. (1988) shows strong, descending inflow to the rear of the convective line at least in the vicinity of the Wichita, Kansas, area (along AA′) as early as 0139.

By 0600 (Fig. 16) deep and extensive rear inflow is analyzed along AA′. The analysis of single Doppler radar data taken in a three-dimensional conical scan mode by Rutledge et al. (1988) provides direct evidence of descending motion in the rear-inflow jet along AA′. Their 0350–0529 time series of vertical velocity at CP-4 (the southern Doppler radar in Kansas; Fig. 3), when projected onto AA′ from 160 to 225 km behind the leading convective line (which extends back to the wake low center), shows sinking motion below 3.5 km MSL with a maximum vertical velocity amplitude of ~0.6 m s^{-1} near 2.5 to 3.0 km MSL. This sinking motion extends through the entire depth of the rear-inflow jet. Further evidence of subsidence can be inferred from slope of the rear-inflow jet, the strength of the flow and the degree of low-level warming and drying. Estimates of the maximum slopes along AA′ and CC′ (the accuracy of which depends on the horizontal resolution of the data) at 0600 are 1:20, considerably greater than

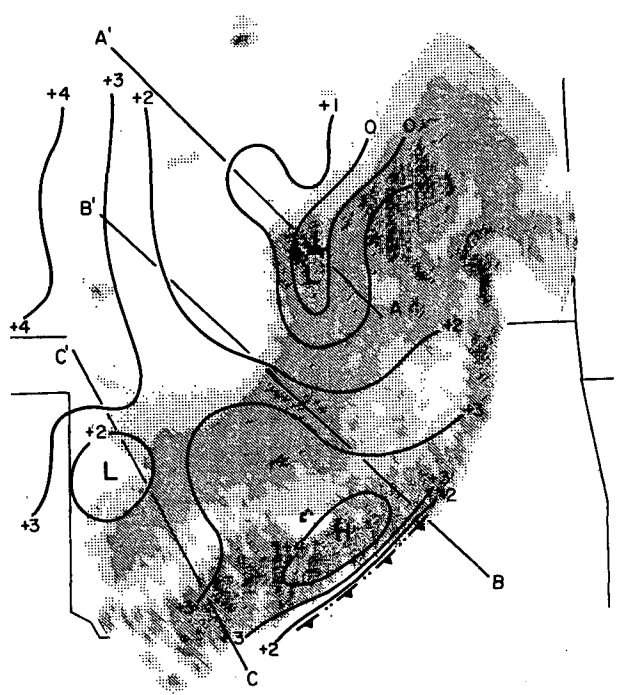

FIG. 15. Positions of three cross sections AA′, BB′ and CC′ illustrated in Fig. 16. Reflectivity field is at 0600 with thresholds of 15, 25, 35 and 50 dBZ. Contours are departures, in mb, of 518 m pressure from 950 mb.

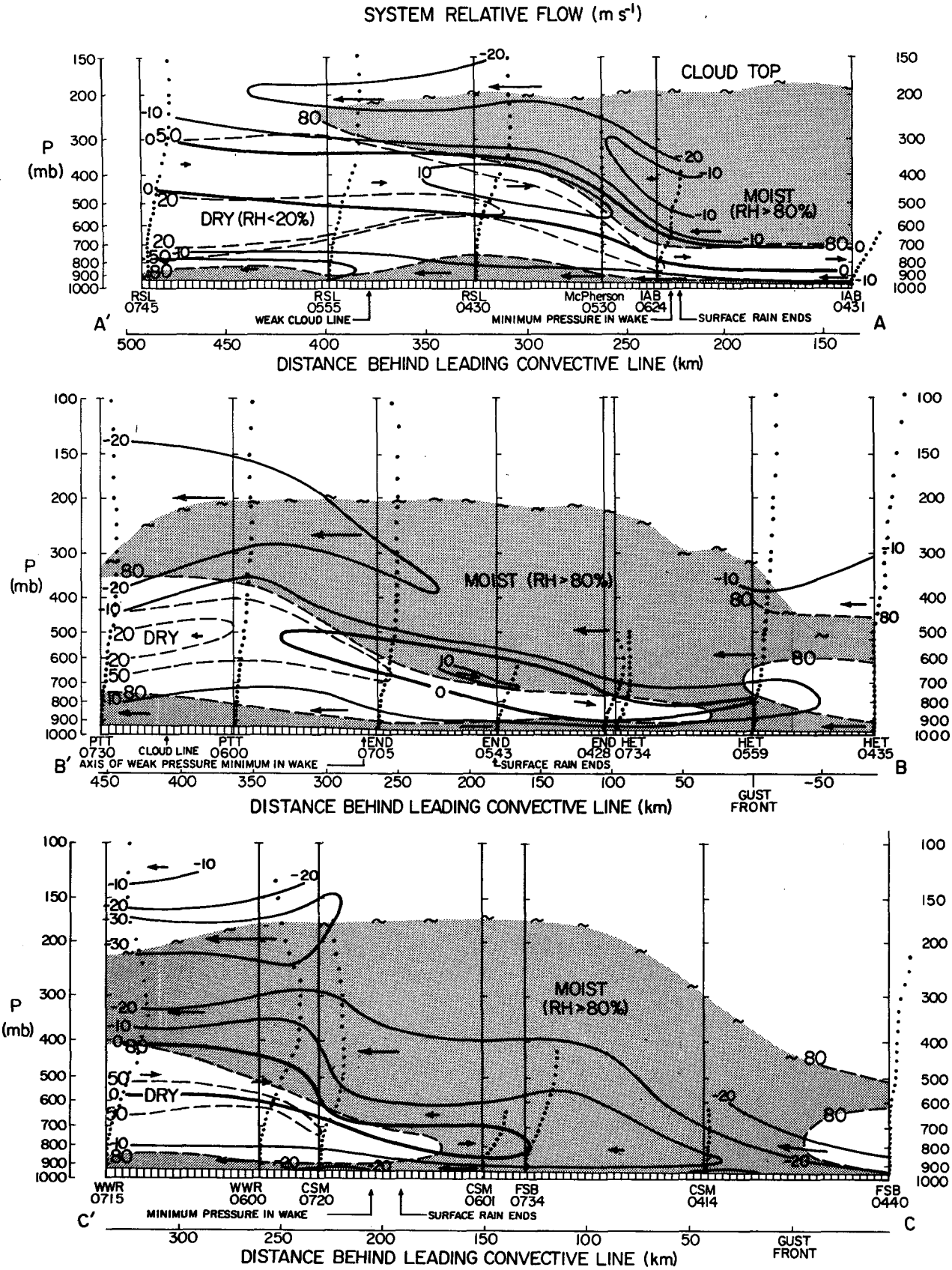

FIG. 16. Composite cross sections of system relative flow (m s^{-1}) and relative humidity (%, with respect to ice at temperatures below freezing) at 0600 UTC 11 June, along AA', BB' and CC' in Fig. 15. Relative humidity greater than 80% is shaded. Cloud top is estimated from infrared satellite data assuming blackbody conditions. Sounding data points (e.g., balloon tracks) are indicated by dots. Data from McPherson are from wind profiler.

that for BB′ (1:50). The rearward extension of the rear-inflow jet behind the stratiform cloud system is notably reduced in the BB′ section, as is the implied subsidence in the vicinity of the wake low. In addition, dry air extends to lower levels along AA′ and CC′ (50% relative humidity down to 850 and 770 mb, respectively) than BB′ (50% at 700 mb). These findings suggest that the weakness in the wake low along BB′ may be a consequence of reduced subsidence there. Further analysis of the relative intensity of subsidence at various positions along the back edge of the squall line is in progress (using kinematically-derived vertical motions based on rawinsonde data) and will be reported in a future paper. The pronounced warming and drying at low levels is clearly evident in the "onion-shaped" soundings prevalent in this region (Zipser 1977; Ogura and Liou 1980; Leary and Rappaport 1987). A good example along AA′ is shown in Fig. 17 for IAB at 0624. Warming and drying there is a maximum at 850 mb or 1 km above the surface, as has been observed in tropical squall lines (Fig. 8 of Zipser 1977).

The horizontal distribution of drying at 850 mb is illustrated in Fig. 18. The driest air is along the back edge of the stratiform region with a pronounced dry pocket at the northern wake low position. Bands of nearly saturated air at this level are analyzed along the leading convective line and about 100 km to the rear of the stratiform rain area where a few isolated showers exist. Warm air at 850 mb is also observed at the back edge (Fig. 19) with the warmest air coincident with the dry anomaly center in Fig. 18. This position also coincides with the northern wake low center and is consistent hydrostatically (observing that the air is several degrees Celsius warmer in the lower troposphere) with the fact that the pressure in this wake low is ~2 mb lower than that in the wake low to the southwest (Fig. 14).

Additionally in Fig. 19, two cold pools are observed at 850 mb behind the leading convective line. These

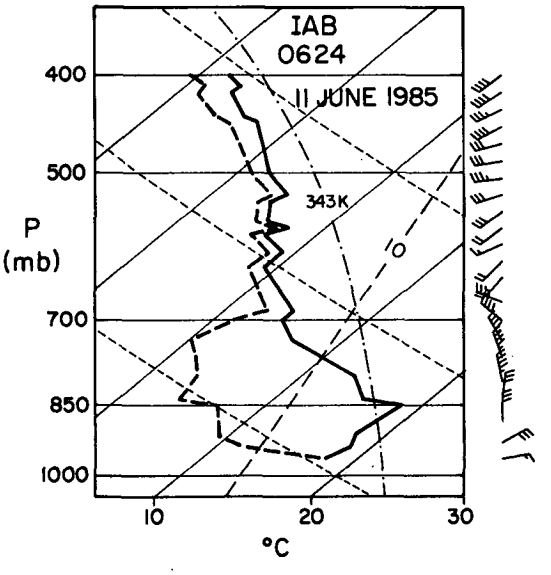

FIG. 17. Skew-T diagram for Wichita, Kansas (IAB) at 0624 UTC 11 June 1985.

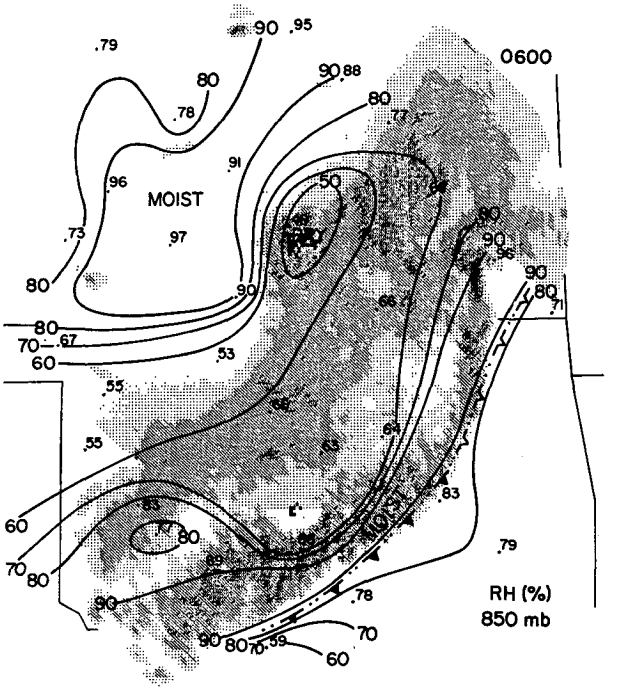

FIG. 18. Composite relative humidity at 850 mb at 0600. Reflectivity thresholds are 15, 25, 35 and 50 dBZ.

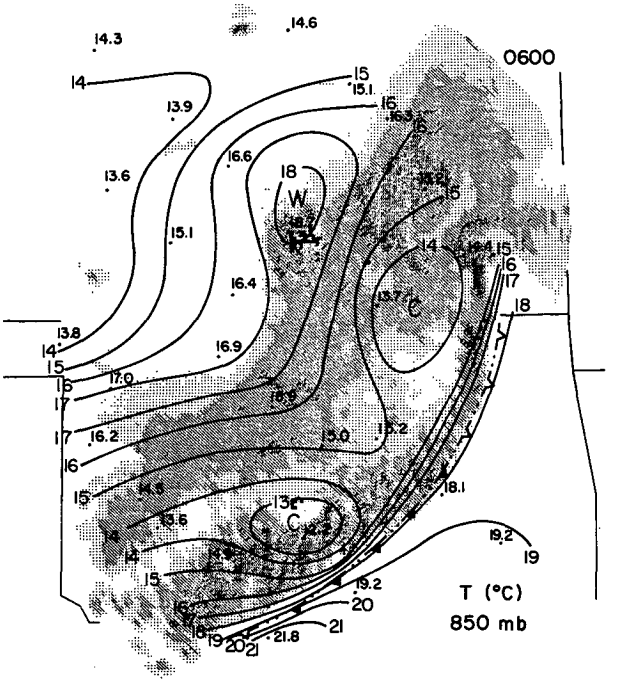

FIG. 19. As in Fig. 18, except for temperature at 850 mb (°C).

features are also evident at 900 mb or 0.5 km (not shown) and probably depict the upper portion of the surface mesohigh cold dome. The warm intrusion between the two centers may represent the effects of the advancing and descending rear-inflow jet. The low-level drying in this area (coinciding with the transition zone minimum of reflectivity and rainfall rate) just behind the convective line can be seen in the relative humidity analysis at 900 mb (Fig. 20). Bands of dry air at the rear of the stratiform region and moist air farther to the rear are evident at 900 mb as they are at 850 mb.

Analogous banded structure in the thermodynamic field can be seen at 700 mb (Figs. 21 and 22). At this level the dry zone behind the stratiform region (Fig. 21) is shifted farther to the rear (as is evident from Fig. 16) and a strong gradient exists along the back edge where strong erosion of the precipitation echo is evidently occurring (also suggested for an Oklahoma squall line studied by Smull and Houze 1985). The entire radar echo area is moist at this level as well as the area along the weak cloud line to the rear of the squall line. The temperature field at 700 mb (Fig. 22) exhibits a warm zone just to the rear of the stratiform area and a large cool anomaly within it. The cooling in the precipitation area can be attributed to melting and evaporation.

The horizontal wind field at four levels is shown in Fig. 23. At the surface (Fig. 23a) a diffluence axis is observed beneath the trailing stratiform region and a confluence line along its back edge. The surface diffluence axis was not always centered in the stratiform region; rather, it was in the transition zone at 0300 and migrated rearward as the squall line matured and stratiform precipitation region intensified. The 0600 composite wind field at 900 mb (Fig. 23b) shows a sharp

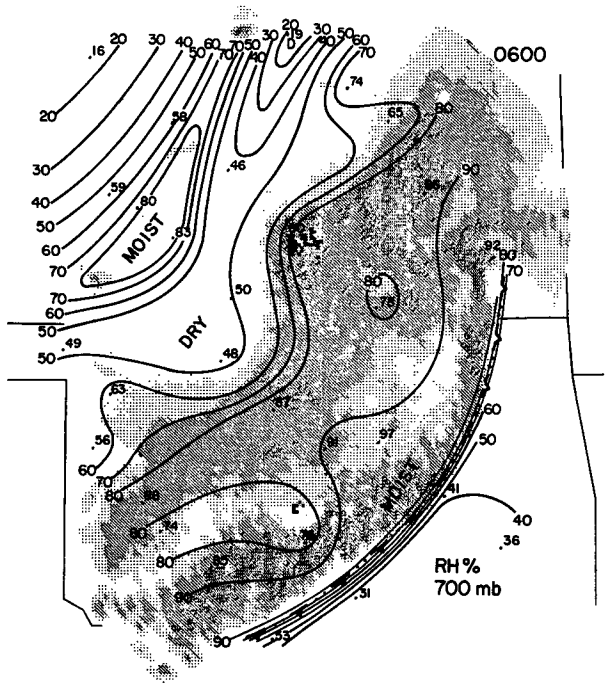

FIG. 21. As in Fig. 18, except for relative humidity at 700 mb.

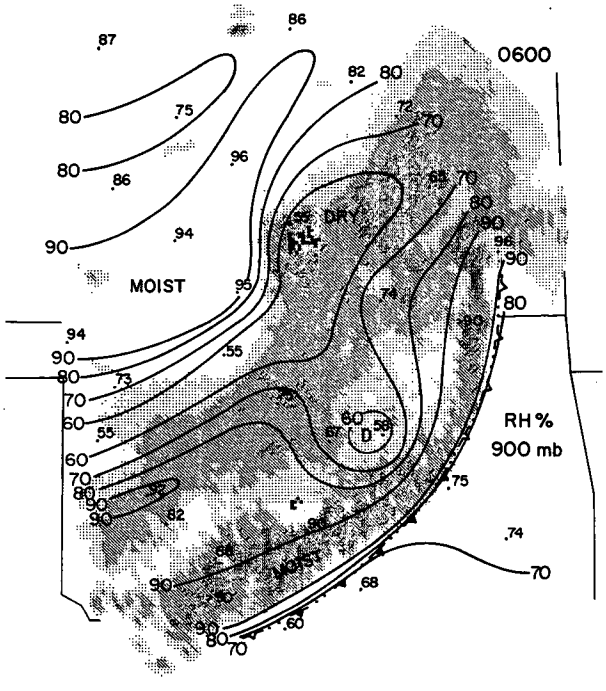

FIG. 20. As in Fig. 18, except for relative humidity at 900 mb.

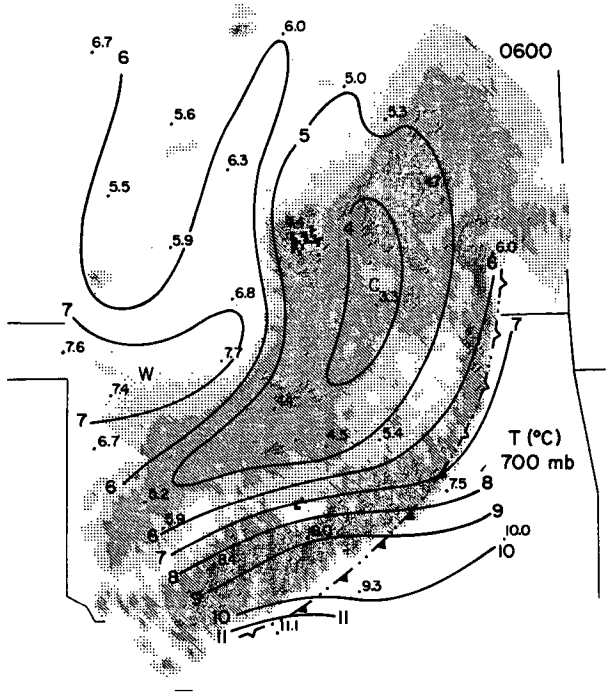

FIG. 22. As in Fig. 18, except for temperature (°C) at 700 mb.

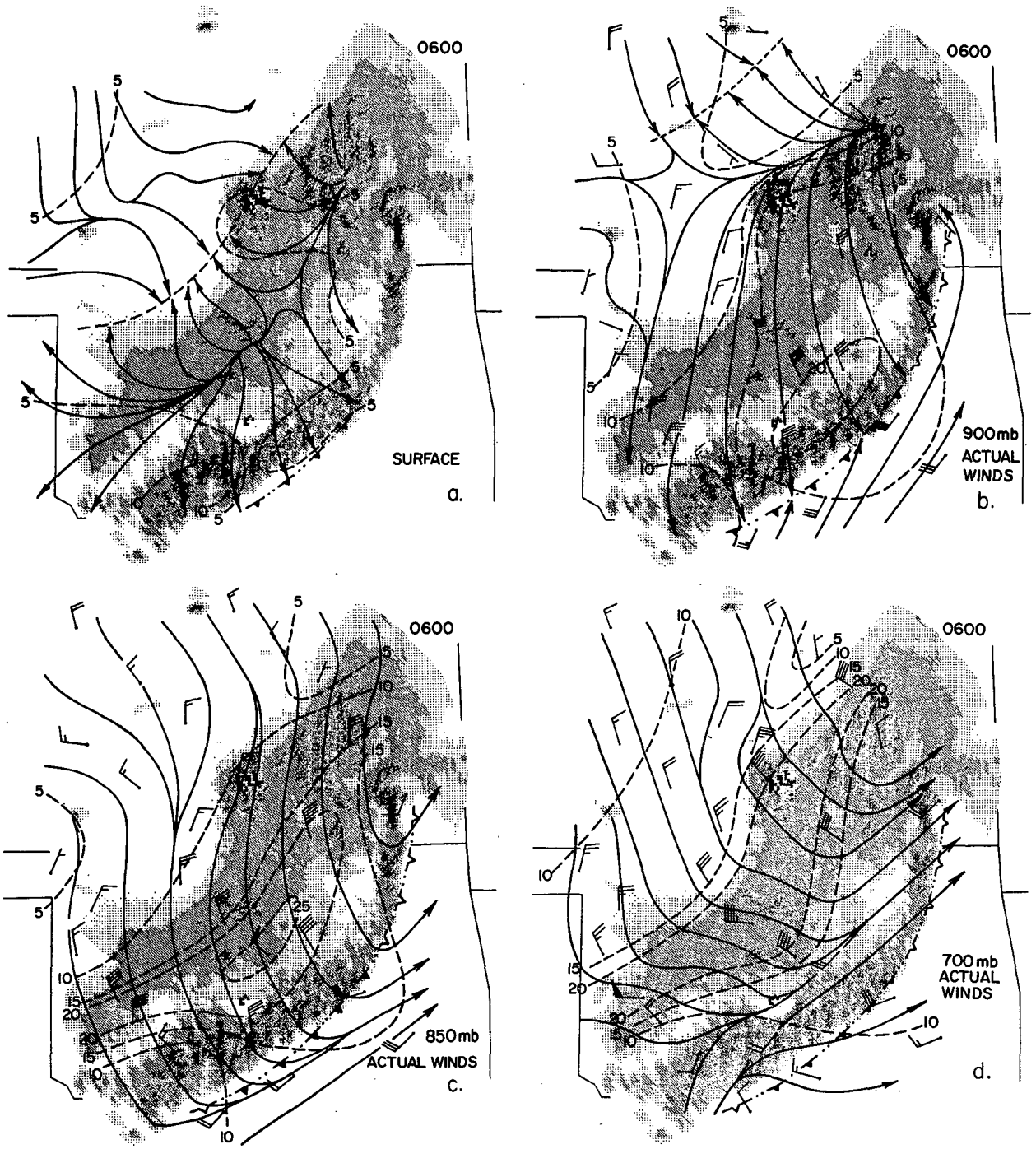

FIG. 23. Composite winds and isotachs (m s^{-1}) at surface (a), 900 mb (b), 850 mb (c) and 700 mb (d) at 0600.

rearward shift of the diffluence and confluence axes with strong divergence indicated in the northern wake low area, consistent with the earlier inference of strong subsidence in this region. The convergence line at 900 mb to the rear of the squall line may be forcing the weak cloud line there; however, its growth appears to be retarded by a very dry and stable layer in this region at the base of the rear-inflow jet near 500–600 mb (Fig. 16). A similar behavior was noted by Koch and McCarthy (1982) in a study of a dryline-initiated mesoscale convective system. The diffluence axis is not seen at 850 or 700 mb (Figs. 23c, d). At these levels the flow is characterized by broad trough-like features. The rear-inflow jet (identified by an elongated region

of maximum wind speed at each level) can be seen sloping down from the stratiform region at 700 mb (Fig. 23d) to 100 km behind the gust front at 850 mb (Fig. 23c) to 50 km behind the gust front at 900 mb (Fig. 23b). This jet is well defined in the storm-relative flow at 700 mb (Fig. 24), a level that cuts sharply across the sloping jet core (Fig. 16). It is clear from Fig. 24 that the flow at 700 mb consists of three distinct currents: a front-to-rear jet, the rear-inflow jet and the front-to-rear lower tropospheric outflow. The warm and dry zone just behind the stratiform region (Figs. 21 and 22) is in the front-to-rear outflow area, suggesting that air from just above this location is descending out of the rear-inflow jet and then flowing back out of the storm. The relative flow in the rear-inflow jet region has a significant along-line component in the southern portion of the area. This complex flow structure suggests that there may be important limitations to a two-dimensional interpretation of certain aspects of the squall line dynamics.

8. Physical processes in the wake low

Evidence presented so far indicates that the wake low in the 10–11 June OK PRE-STORM squall line went through the evolutionary phases described by Fujita (1963, Fig. 1) and Pedgley (1962). However, with the case studied here, there is additional information concerning the relationship of the wake low to the stratiform precipitation region of the squall line and its adjacent rear-inflow circulation. In particular, it appears as though there is a very close association between the development of the wake low and the development of the stratiform region during the squall life cycle. With these findings, we can provide supplementary information to the four stages identified by Fujita (1963):

1) *Initiation stage.* A small mesohigh forms and develops in association with deep convection along the squall line. No wake low is present and the trailing stratiform precipitation area is weak (several hours prior to Fig. 13a).

2) *Development stage.* Horizontal dimensions of the line increase to over 150 km, yet no well-defined wake low appears inside the system. The stratiform area behind the leading convective line has expanded, but no distinct reflectivity maximum in this area has developed (Fig. 13b).

3) *Mature stage.* Convective showers reach or have passed their maximum intensities, and an enhancement of the trailing stratiform precipitation region develops parallel to and separated from the leading convective line, with a wake low centered along the back edge of the enhanced stratiform region (Fig. 13c and d).

4) *Dissipation stage.* The wake low reaches minimum deficit pressure and convective showers disintegrate. The trailing stratiform precipitation maximum begins to break up and weaken, but the wake low continues to "hug" its back edge (Fig. 13e).

This description of the life cycle corresponds reasonably well with the growth, mature and decay stages of a squall line defined by Pedgley (1962); however, we have given slightly greater emphasis to the relationship between the stratiform precipitation area and the wake low throughout the entire life cycle.

The positioning of the wake low at the back edge of the stratiform precipitation area and the existence of a descending rear-inflow jet crossing this line, suggests a physical link between the wake low and the rear-inflow jet. A schematic illustrating this association is presented in Fig. 25a. Outside the stratiform rain area a descending, midtropospheric rear-inflow jet is observed. Maximum warming and drying appear near 1 km AGL (850 mb) just to the rear of the light precipitation region. The minimum pressure occurs at this position and can be explained hydrostatically as a direct result of the warming (Williams 1963). As the descending jet enters the rain area, strong evaporative cooling and moistening significantly offset the subsidence warming and drying and, consequently, the surface pressure reduction is less. Sublimation and evaporative cooling also occur aloft to the rear of the wake low; however, the cooling rate is presumably less due to the lower precipitation rate.

The close proximity of the wake low to the stratiform region further suggests that the stratiform cloud system itself may be directly responsible for generating a mesoscale circulation in its immediate vicinity, as has been

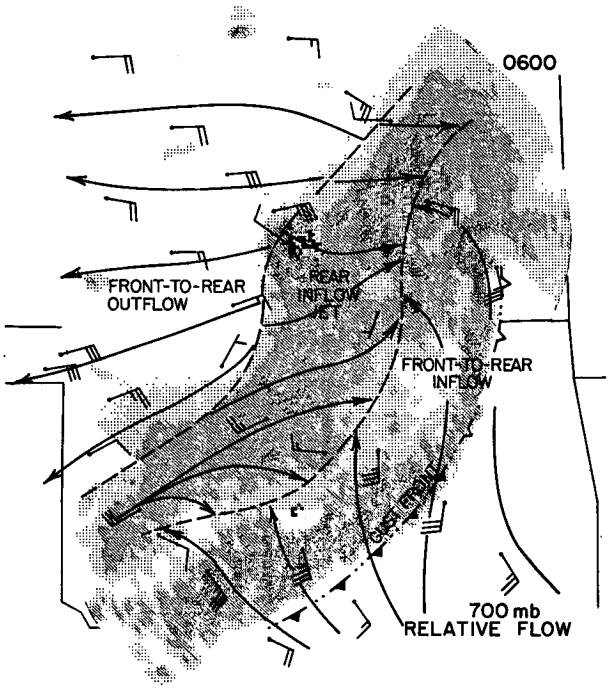

FIG. 24. System-relative composite winds at 700 mb at 0600.

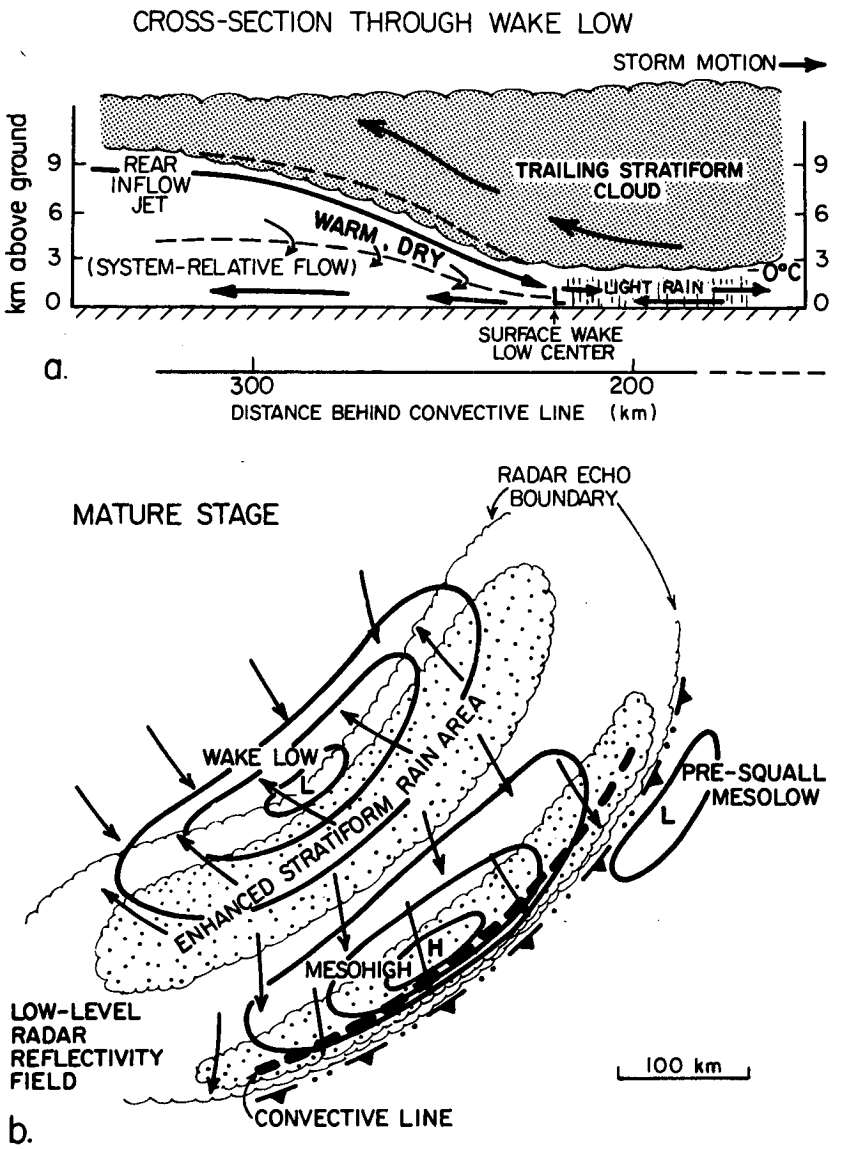

FIG. 25. Schematic cross section through wake low (a) and surface pressure and wind fields and precipitation distribution during squall line mature stage (b). Winds in (a) are system-relative with the dashed line denoting zero relative wind. Arrows indicate streamlines, not trajectories, with those in (b) representing actual winds. Note that horizontal scales differ in the two schematics.

shown by Brown (1979). An analysis of the composite geopotential height field at 0600 (to be reported in a later paper) indicates a pronounced mesolow with maximum amplitude just above the 0°C level centered in the trailing stratiform region (with a peak intensity in the northern stratiform precipitation maximum). A recent modeling study by Szeto et al. (1988) indicates that both melting and evaporation in the stratiform rain area are important in generating a descending current adjacent to the stratiform region. The centering of the wake lows behind the two stratiform segments (Fig. 13e), suggests a possible physical link between the two features. Indeed, the dual splitting of the wake low and stratiform areas could conceivably be explained by the generation of a midtropospheric mesolow in the stratiform region (Brown 1979) and the possible subsequent development of a rear-inflow jet (as proposed by Smull and Houze 1987b). If the intensity of a descending rear-inflow jet is directly proportional to the intensity of the stratiform precipitation, then subsidence warming and hydrostatic lowering of the surface pressure should be maximized at those locations, where stratiform precipitation is strongest.

Another revision to Fujita's (1955) depiction of the surface features (Fig. 1) accompanying a squall line with trailing stratiform precipitation pertains to the flow

field in the vicinity of the wake low (Fig. 25b). Fujita's schematic illustrates airflow into the center of the low, as might be expected for a stationary, long-lived pressure pattern. However, the data from our PRE-STORM analyses, as well as that presented in numerous case studies by Williams (1953) and Fujita (1955, 1963), indicate that the axis of surface confluence in the wake low area occurs 20 to 50 km behind the low center, not in the center itself. This situation can be ascribed to the highly transient nature of the pressure field (Garratt and Physick 1983). With respect to the surface air behind the squall line, the wake low propagated rapidly to the east. Therefore, surface air parcels were exposed to intense pressure gradients and accelerations for only short periods of time as the mesolow passed and, as in the case of the mesohigh, there are regions where the flow is actually in the direction of higher pressure.

9. Summary and conclusions

Data from the Oklahoma–Kansas PRE-STORM on 10–11 June 1985 have been used to determine the relationship of the surface pressure features in an intense midlatitude squall line to its precipitation and airflow structure. In general, three main features in the pressure field are evident: 1) a mesolow preceding the squall line, 2) a mesohigh immediately to the rear of the leading convective line and 3) a wake low at the back edge of the trailing stratiform region. Particular attention has been given in this study to the wake low, its life cycle and association with the trailing stratiform portion of the squall line.

In the formative stage of the line the pressure field to the rear of the convectively-induced squall line mesohigh is relatively flat with only weak stratiform precipitation present. During the developing-to-mature stages of the squall line, a trailing stratiform region forms and a pronounced wake low appears at its back edge. The maximum low-level reflectivity in the trailing stratiform region at this time is separated from the convective line by a transition zone (Chong et al. 1987; Smull and Houze 1987a). During this period, the lowest pressure appears to occur in the region of a "notch" (Smull and Houze 1985) in the reflectivity pattern at the trailing edge of the line. Strong, descending rear-inflow into the back of the convective line had also developed during this period (Rutledge et al. 1988).

Surface precipitation data have permitted an estimate to be made of the total squall line rainfall attributable to the stratiform region. Based on 5-minute data from the NCAR PAM II and NSSL SAM stations, it is estimated that 29% of the surface precipitation intercepted by the mesonetwork area (covering much of central Kansas and Oklahoma) is from the stratiform component. This value agrees well with the 30 to 40% estimates from tropical squall line studies (Houze 1977; Cheng and Houze 1979; Houze and Rappaport 1984; Leary 1984; Churchill and Houze 1984; Wei and Houze 1987).

During the mature-to-dissipating stages of the squall line, the trailing stratiform region splits into two segments. The wake low also splits in two at this time with each center positioned at the back edge of the two stratiform segments. The split is possibly related to the penetration of the rear-inflow jet into the stratiform precipitation region, such that 1) strong subsidence partially dissipates the stratiform cloud system and 2) increased evaporative cooling in the jet weakens the low-level subsidence warming and the intensity of the wake low. The mesohigh continues as a single center on a relatively steady track to the southeast between the two wake lows. A composite analysis of rawinsonde data at this time shows strong warming and drying centered near 1 km AGL (850 mb in our case) at the back edge of the stratiform region. The strongest warming and drying is located at the position of the most intense wake low.

Based on the results of this study it is proposed that the wake low, which can be attributed to subsidence warming (Williams 1963; Zipser 1977), is a surface manifestation of the descending rear-inflow jet and that the warming is maximized at the back edge of the precipitation area where there is insufficient evaporative cooling to offset strong adiabatic warming (Fig. 25). Because the wake low "hugs" the back edge of the stratiform area, it appears as though processes in the stratiform precipitation region itself may be responsible for contributing in an important way to the adjacent descending rear inflow (as suggested by Smull and Houze 1987b and Szeto et al. 1988).

Acknowledgments. We extend our thanks to James Toth for his considerable assistance throughout this study. We also thank Drs. David Jorgensen and Bradley Smull for their help in radar data processing, and William Gallus, Gregory Stumpf, Tammy Taylor and Jeff Zimmerman for their contributions to the analysis. Comments on a draft by Profs. William Cotton, Robert Houze and Steven Rutledge and Dr. Bradley Smull, and on the submitted manuscript by two anonymous reviewers have been very helpful. The NCAR Field Observing Facility staff provided exceptional support to the operation of the PAM II mesonetwork during OK PRE-STORM. The surface analyses were completed with the aid of NASA's GEMPAK software. This research has been supported by the National Science Foundation, Atmospheric Sciences Division, under Grant ATM-8507961.

APPENDIX

Corrections to PAM/SAM Pressure Data

Pressure at the PAM sites was measured with the NCAR aneroid barometer at 2 m above the ground. Field calibration at each PAM site was conducted two

to three times throughout the experiment and in some instances errors of up to 1 to 2 mb were noted. In order to produce corrections to the pressure dataset, three sources of information were used: 1) the NCAR barometer calibration records, 2) analyses of monthly mean maps of pressure in the PAM array and 3) pressure data from interior National Weather Service stations. The monthly mean maps (shown in Johnson and Toth 1986) were completed following the filling of the very few (2%) gaps in the PAM pressure data. Before analysis, pressures were first adjusted to 500 m, the approximate mean elevation of all stations, using an average layer mean virtual temperature of 293 K for 1–21 May and 297 K for 21 May–31 June. The 500 m average pressures revealed for May and June, as might be expected for a long term average, a weak eastward-directed pressure gradient (1 to 2 mb, supporting a southerly geostrophic wind) across the domain. Using the well-calibrated NWS stations to tie down the pressure field at several points, a smooth subjective analysis was then conducted. During this process, individual station pressures were adjusted so that a smooth field could be obtained. The resulting adjustments to station pressure agreed extremely well with the NCAR calibration-determined pressure corrections, except at three stations (P5, P15 and P28). The disagreement at these stations was felt to be a consequence of inaccurate estimates of elevation at those sites and, based on this pressure adjustment information, the elevations at those stations were corrected.

The NSSL SAM pressures were calibrated at each site approximately once a week. The same correction

TABLE 1. PAM/SAM station pressure corrections.

Station	Elevation (m)	Applied pressure correction (mb)	Station	Elevation (m)	Applied pressure correction (mb)
P01	799	+1.3	S01	358	+0.6
P02	651	+0.9	S02	530	+0.8
P03	575	−0.5	S03	435	+2.2
P04	540	−1.2	S04	412	+1.8
P05	484	0.0	S05	394	+0.8
P06	404	−0.1	S06	377	+1.0
P07	452	+0.8	S07	331	+0.1
P08	461	−0.6	S08	383	+0.1
P09	791	−0.2	S09	207	+0.6
P10	653	−0.3	S10	681	M
P11	613	−0.2	S11	527	M
P12	545	+1.1	S12	474	+1.9
P13	479	+0.7	S13	433	+1.4
P14	467	−2.2	S14	350	M
P15	403	+1.0	S15	384	−0.3
P16	371	+0.2	S16	314	+0.2
P17	821	−0.1	S17	293	+0.6
P18	725	−0.1	S18	817	−0.3
P19	632	+0.4	S19	661	M
P20	561	−0.2	S20	516	+1.3
P21	472	+0.4	S21	464	M
P22	407	−0.7	S22	418	+1.1
P23	418	+0.3	S23	380	+0.5
P24	336	−0.4	S24	302	M
P25	769	+0.1	S25	256	+0.5
P26	625	0.0	S26	789	0.0
P27	625	−0.1	S27	696	+0.4
P28	530	−1.8	S28	594	M
P29	434	+1.4	S29	480	+1.2
P30	387	+0.8	S30	328	+0.4
P31	407	1.4	S31	316	+1.5
P32	320	M	S32	293	M
P33	786	−0.1	S33	287	−0.3
P34	628	+0.3	S34	809	+0.4
P35	546	0.0	S35	648	M
P36	379	+0.2	S36	567	+0.9
P37	356	+0.5	S37	395	+0.6
P38	330	+0.2	S38	414	+1.8
P39	374	+2.0	S39	305	+0.8
P40	300	E +1.1	S40	309	M
P41	414	E −0.7	S41	248	+1.9
P42	480	E +0.2	S42	331	+0.2

E: Estimated; M: Missing.

procedures that were applied to the PAM data, however, could not be applied to the SAM data because of a much higher frequency of missing observations. An alternate procedure was used that took advantage of the interior and adjacent well calibrated NWS pressure data. Using only NWS station data, a smooth subjective analysis of 441 m (the average elevation of SAM stations) pressure was conducted at 2100, 2200 and 2300 UTC 10 June over the SAM array. This period was characterized by southerly flow and very little convection just prior to the arrival of the squall line. From this analysis, pressures were then interpolated to the SAM sites. The difference between the interpolated pressure and the 441 m SAM adjusted pressure yielded a set of pressure corrections that were subsequently used in the pressure analyses for the 10–11 June squall line.

Table 1 summarizes the pressure corrections used in the 10–11 June analyses. The SAM values have an overall negative bias, which does not have a clear explanation.

REFERENCES

Atkinson, B. W., 1981: *Meso-scale Atmospheric Circulations.* Academic Press, 495 pp.

Augustine, J. A., and E. J. Zipser, 1987: The use of wind profilers in a mesoscale experiment. *Bull. Amer. Meteor. Soc.*, **68**, 4–17.

Bluestein, H. B., and M. H. Jain, 1985: Formation of mesoscale lines of precipitation: Severe squall lines in Oklahoma during the spring. *J. Atmos. Sci.*, **42**, 1711–1732.

Brown, J. M., 1979: Mesoscale unsaturated downdrafts driven by rainfall evaporation: A numerical study. *J. Atmos. Sci.*, **36**, 313–338.

Brunk, I. W., 1953: Squall lines. *Bull. Amer. Meteor. Soc.*, **34**, 1–9.

Byers, H. R., and R. R. Braham, Jr., 1949: *The Thunderstorm.* U.S. Govt. Printing Office, Washington DC, 287 pp.

Cheng, C.-P., and R. A. Houze, Jr., 1979: The distribution of convective and mesoscale precipitation in GATE radar echo patterns. *Mon. Wea. Rev.*, **107**, 1370–1381.

Chong, M., P. Amayenc, G. Scialom and J. Testud, 1987: A tropical squall line observed during the COPT 81 experiment in West Africa. Part 1: Kinematic structure inferred from dual-Doppler radar data. *Mon. Wea. Rev.*, **115**, 670–694.

Churchill, D. D., and R. A. Houze, Jr., 1984: Development and structure of winter monsoon cloud clusters on 10 December 1978. *J. Atmos. Sci.*, **41**, 933–960.

Cunning, J. B., 1986: The Oklahoma–Kansas Preliminary Regional Experiment for STORM-Central. *Bull. Amer. Meteor. Soc.*, **67**, 1478–1486.

Fankhauser, J. C., 1974: The derivation of consistent fields of wind and geopotential height from mesoscale rawinsonde data. *J. Appl. Meteor.*, **13**, 637–646.

Fritsch, J. M., and C. G. Chappell, 1980: Numerical prediction of convectively driven mesoscale pressure systems, II, Mesoscale model. *J. Atmos. Sci.*, **37**. 1734–1762.

Fujita, T. T., 1955: Results of detailed synoptic studies of squall lines. *Tellus*, **7**, 405–436.

——, 1959: Precipitation and cold air production in mesoscale thunderstorm systems. *J. Meteor.*, **16**, 454–466.

——, 1963: Analytical mesometeorology. A review. *Meteor. Monogr.*, **5**, 77–125.

Gamache, J. F., and R. A. Houze, Jr., 1982: Mesoscale air motions associated with a tropical squall line. *Mon. Wea. Rev.*, **110**, 118–135.

——, and ——, 1983: Water budget of a mesoscale convective system in the tropics. *J. Atmos. Sci.*, **40**, 1835–1850.

——, and ——, 1985: Further analysis of the composite wind and thermodynamic structure of the 12 September GATE squall line. *Mon. Wea. Rev.*, **113**, 1241–1259.

Garratt, J. R., and W. L. Physick, 1983: Low-level wind response to mesoscale pressure systems. *Bound.-Layer Meteor.*, **27**, 69–87.

Houze, R. A., Jr., 1977: Structure and dynamics of a tropical squall-line system. *Mon. Wea. Rev.*, **105**, 1540–1567.

——, and E. N. Rappaport, 1984: Air motions and precipitation structure of an early summer squall line over the eastern tropical Atlantic. *J. Atmos. Sci.*, **41**, 553–574.

Hoxit, L. R., C. F. Chappell and J. M. Fritsch, 1976: Formation of mesolows or pressure troughs in advance of cumulonimbus clouds. *Mon. Wea. Rev.*, **104**, 1419–1428.

Johnson, B. C., 1983: The heat burst of 29 May 1976. *Mon. Wea. Rev.*, **111**, 1776–1792.

Johnson, R. H., and M. E. Nicholls, 1983: A composite analysis of the boundary layer accompanying a tropical squall line. *Mon. Wea. Rev.*, **111**, 308–319.

——, and J. J. Toth, 1986: Preliminary data quality analysis for the Oklahoma-Kansas PRE STORM PAM II mesonetwork. Colorado State University, Atmospheric Science Paper No. 407, 41 pp. [Available from the authors at the Department of Atmospheric Science, Colorado State University, Fort Collins 80523].

Klemp, J. B., and R. B. Wilhelmson, 1978: Simulations of right- and left-moving storms produced through storm splitting. *J. Atmos. Sci.*, **35**, 1097–1110.

Koch, S. E., and J. McCarthy, 1982: The evolution of an Oklahoma dryline. Part II: Boundary-layer forcing of mesoconvective systems. *J. Atmos. Sci.*, **39**, 237–257.

Leary, C. A., 1984: Precipitation structure of the cloud clusters in a tropical easterly wave. *Mon. Wea. Rev.*, **112**, 313–325.

——, and R. A. Houze, Jr., 1979: The structure and evolution of convection in a tropical cloud cluster. *J. Atmos. Sci.*, **36**, 437–457.

——, and E. N. Rappaport, 1987: The life cycle and internal structure of a mesoscale convective complex. *Mon. Wea. Rev.*, **115**, 1503–1527.

LeMone, M. A., 1983: Momentum transport by a line of cumulonimbus. *J. Atmos. Sci.*, **40**, 1815–1834.

Maddox, R. A., 1976: An evaluation of tornado proximity wind and stability data. *Mon. Wea. Rev.*, **104**, 133–142.

Miller, M. J., and A. K. Betts, 1977: Traveling convective storms over Venezuela. *Mon. Wea. Rev.*, **105**, 833–848.

Moncrieff, M. W., and J. S. A. Green, 1972: The propagation and transfer properties of steady convective overturning in shear. *Quart. J. Roy. Meteor. Soc.*, **98**, 336–352.

——, and M. J. Miller, 1976: The dynamics and simulation of tropical cumulonimbus and squall lines. *Quart. J. Roy. Meteor. Soc.*, **102**, 373–394.

Newton, C. W., 1950: Structure and mechanism of the prefrontal squall line. *J. Meteor.*, **7**, 210–222.

——, 1966: Circulations in large sheared cumulonimbus. *Tellus*, **18**, 699–713.

——, and J. C. Fankhauser, 1964: On the movements of convective storms, with emphasis on size discrimination in relation to water-budget requirements. *J. Appl. Meteor.*, **3**, 651–688.

Ogura, Y., and M. T. Liou, 1980: The structure of a mid-latitude squall line: A case study. *J. Atmos. Sci.*, **37**, 553–567.

Pedgley, D. E., 1962: A meso-synoptic analysis of the thunderstorms on 28 August 1958. *Brit. Meteor. Off., Geophys. Mem.*, **No. 106**, 74 pp.

Purdom, J. F. W., 1976: Some uses of high-resolution GOES imagery in the mesoscale forecasting of convection and its behavior. *Mon. Wea. Rev.*, **104**, 1474–1483.

Rotunno, R., J. B. Klemp, and M. L. Weisman, 1988: A theory for squall lines. *J. Atmos. Sci.*, submitted.

Rutledge, S. A., 1986: A diagnostic modeling study of the stratiform region associated with a tropical squall line. *J. Atmos. Sci.*, **43**, 1356–1377.

——, and R. A. Houze, Jr., 1987: A diagnostic modeling study of the trailing stratiform region of a midlatitude squall line. *J. Atmos. Sci.*, **44**, 2640–2656.

——, ——, M. I. Biggerstaff and T. Matejka, 1988: The Oklahoma–Kansas mesoscale convective system of 10–11 June 1985: Precipitation structure and single-Doppler radar analysis. *Mon. Wea. Rev.*, in press.

Sanders, F., and R. J. Paine, 1975: The structure and thermodynamics of an intense storm in Oklahoma. *J. Atmos. Sci.*, **32**, 1563–1579.

——, and K. A. Emanuel, 1977: The momentum budget and temporal evolution of a mesoscale convective system. *J. Atmos. Sci.*, **34**, 322–330.

Sawyer, J. S., 1946: Cooling by rain as a cause of the pressure rise in convective squalls. *Quart. J. Roy. Met. Soc.*, **72**, 168.

Schaefer, J. T., L. R. Hoxit and C. F. Chappell, 1985: Thunderstorms and their mesoscale environment. *Thunderstorm Morphology and Dynamics*, Edwin Kessler, Ed., 113–130.

Smull, B. F., and R. A. Houze, Jr., 1985: A midlatitude squall line with a trailing region of stratiform rain: Radar and satellite observations. *Mon. Wea. Rev.*, **113**, 117–133.

——, and ——, 1987a: Dual-Doppler radar analysis of a mid-latitude squall line with a trailing region of stratiform rain. *J. Atmos. Sci.*, **44**, 2128–2148.

——, and ——, 1987b: Rear inflow in squall lines with trailing stratiform precipitation. *Mon. Wea. Rev.*, **115**, 2869–2889.

Srivastava, R. C., T. J. Matejka and T. J. Lorello, 1986: Doppler radar study of the trailing anvil region associated with a squall line. *J. Atmos. Sci.*, **43**, 356–377.

Szeto, K. K., R. E. Stewart and C. A. Lin, 1988: Mesoscale circulations forced by melting snow. Part II. Application to meteorological features. *J. Atmos. Sci.*, **45**, 1642–1650.

Wei, T., and R. A. Houze, Jr., 1987: The GATE squall line of 9–10 August 1974. *Advances in Atmospheric Sciences*, **4**, 85–92.

Weisman, M. L., and J. B. Klemp, 1982: The dependence of numerically simulated convective storms on vertical wind shear and buoyancy. *Mon. Wea. Rev.*, **110**, 504–520.

Williams, D. T., 1953: Pressure wave observations in the central midwest, 1952. *Mon. Wea. Rev.*, **81**, 278–298.

——, 1963: The thunderstorm wake of May 4, 1961. Natl. Severe Storms Project Rep. No. 18, U.S. Dept. of Commerce, Washington DC, 23 pp. [NTIS PB 168223].

Zipser, E. J., 1969: The role of organized unsaturated downdrafts in the structure and rapid decay of an equatorial disturbance. *J. Appl. Meteor.*, **8**, 799–814.

——, 1977: Mesoscale and convective-scale downdrafts as distinct components of squall-line circulation. *Mon. Wea. Rev.*, **105**, 1568–1589.